Unified description of odd-mass indium nuclei I. General theory and comparison to ^{113}In and ^{115}In levels populated in the decay of ^{113}Sn and ^{115}Cd^{m,g} †

K. Heyde and M. Waroquier*
Laboratorium voor Kernfysika, Proeftuinstraat 86, B-9000 Gent, Belgium

R. A. Meyer
Lawrence Livermore Laboratory, University of California, Livermore, California 94550
(Received 14 June 1977)

We describe the rich variety of nuclear phenomena in the odd-mass indium isotopes by taking into account the coupling of both single-hole and one-particle two-hole configurations (seniority $v = 1$ and $v = 3$) with the quadrupole and octupole vibrations of the underlying core (Sn) nucleus. To fully test the calculations, we have performed detailed spectroscopic studies of the ^{113}Sn, ^{115}Cd^m, and ^{115}Cd^g decays. Energy spectra, spectroscopic factors for stripping and pickup reactions, and electromagnetic properties are calculated and compared with the experimental results for ^{115}In. We compare our model with earlier calculations for the odd-mass In isotopes and with band-mixing calculations using a deformed basis (Nilsson model) for all odd-mass In isotopes ($107 \leq A \leq 119$). The equivalence of the unified-model description with a rotational interpretation is discussed in some detail.

[NUCLEAR STRUCTURE, RADIOACTIVITY Unified-model calculation; chemically separated sources; measured E_γ, I_γ; deduced ^{115}In and ^{113}In levels; Compton suppression.]

I. INTRODUCTION

Attempts to explain the nuclear structure of the odd-mass In isotopes by either spherical hole-core coupling or deformed (Nilsson model) descriptions have encountered many difficulties. Hole-core coupling calculations can explain the single-hole excitations $1g_{9/2}^{-1}$, $2p_{1/2}^{-1}$, and $2p_{3/2}^{-1}$ and the one quadrupole phonon multiplet $|1g_{9/2}^{-1}2_1^+; JM\rangle$ quite well.[1-6] However, hole-core coupling calculations cannot explain:

(i) rather strong $B(M1)$ transitions from levels in the vicinity of the $|g_{9/2}^{-1}2_1^+\rangle$ multiplet energy to the $J^\pi = \frac{9}{2}^+$ ground state,[7,9]
(ii) a set of "extra" low-lying ($E_x \approx 1$ MeV) $J^\pi = \frac{1}{2}^+, \frac{3}{2}^+, \ldots, \frac{9}{2}^+$ levels in the energy region corresponding to the $|1g_{9/2}^{-1}2_1^+; JM\rangle$ multiplet,[10-19]
(iii) strongly enhanced $B(E2; \frac{1}{2}_1^+ \rightarrow \frac{3}{2}_1^+)$ [$\approx$100 Weisskopf units (W.u.)] and $B(E2; \frac{7}{2}_1^+ \rightarrow \frac{3}{2}_1^+)$ ($\approx$55 W.u.) values[8,9] in ^{115}In,
(iv) the large quadrupole moment of the $J^\pi = \frac{3}{2}_1^+$ level,[20,21] and
(v) studies of the reactions ^{112,114,116}Cd(τ, d)-^{113,115,117}In clearly indicating that the levels populated are due mainly to one-particle–two-hole (1p-2h) excitations through the $Z = 50$ proton closed shell.[22-25]

Several attempts have been made to incorporate these extra levels in the hole-core coupling calculations in a rather *ad hoc* way as being due to rotational excitations built on the $\frac{1}{2}^+[431]$ Nilsson orbital.[2,4] Recently, a calculation has been performed in which hole-core ($Z = 50$, Sn) configurations and particle-core ($Z = 48$, Cd) configurations have been considered.[5] The major difficulty that arises in these attempts is how to calculate the matrix elements that connect the two subsystems.

Therefore, we have performed a unified-model calculation for the description of the odd-mass In isotopes (especially ^{115}In) without introducing rotational states or the particle-core (Cd) coupled configurations as unspecified states. All single-hole ($1g_{9/2}^{-1}$, $2p_{1/2}^{-1}$, $2p_{3/2}^{-1}$, $1f_{5/2}^{-1}$) and 1p-2h and 1p-2h states [seniority $v = 1$ and $v = 3$ with $p \in (2d_{5/2}, 1g_{7/2}, 3s_{1/2}, 2d_{3/2}, 1h_{11/2})$] are considered, together with the collective excitations of the underlying Sn core (quadrupole as well as octupole phonons). We perform the calculation in a two-step procedure: First, we treat the Cd nuclei in a hole-core (Sn) coupling calculation. Afterward, we treat simultaneously the hole-core (Sn) and particle-core (Cd) configurations and therein show the precise structure of the Cd-core states and their relations with the hole-core (Sn) configurations.

This two-step procedure and the Hamiltonian[26-28]

used are discussed in Sec. IV. We also discuss the simplification toward the numerically simpler hole-core (Sn) plus particle-core (Cd) calculation and point out the limited validity of the assumptions for these calculations as they were performed by Abecasis, Civitarese, and Krmpotic.[5] Parameters and truncation effects are also discussed.[29-36]

These results for ^{115}In that concern energy spectra, spectroscopic factors, and electromagnetic properties for both stripping and pickup reactions are given in Sec. V and compared with experimental data[30-32,37-40] and with earlier calculations. The unified model is compared with a rotational explanation[41-46] for the $J^\pi = \frac{1}{2}^+, \frac{3}{2}^+, \ldots$ sequence of levels, and the strong resemblance between this aspect of the two theories is pointed out. In Sec. VI we discuss our calculations and parameters[47-53] for a deformed basis (Nilsson model) in order to look for an alternative description for the "intruder" states. The idea of coexistence between spherical and deformed states in the odd-mass In isotopes is discussed. A complete band-mixing calculation for all $N = 4$ harmonic-oscillator Nilsson orbitals, corresponding to the equilibrium deformation for the $\frac{1}{2}^+[431]$ orbital, is performed and compared with the experimental results and with earlier attempts at describing these low-lying ($0.5 < E_x < 1.5$ MeV) positive-parity states as members of a pure rotational band on top of the $\frac{1}{2}^+[431]$ Nilsson orbital.

The published data on ^{115}In electromagnetic transitions in the decay of the ^{115}Cd isomers[54,55] have remained essentially the same as published by Graffee *et al.*[56] Improvements on the specific level and transition properties have been reported.[57-60] Here we report our measurements based on advanced spectroscopy techniques[61,62] that have allowed us to detect a number of interlevel transitions in ^{115}In and rectify a number of errors in earlier works.[9,54] We have made preliminary reports of these results elsewhere.[63-69] We report our final results for the relative intensity measurement of an $E3$ transition between the 391-keV $3p_{1/2}$ level and the $1g_{9/2}$ ground state in ^{113}In and for identification of population of the $\frac{1}{2}^+$ level at 1029.7 keV in ^{113}Sn decay.[64,70,71] Heavy-ion Coulomb excitation[72] tends to verify this $E3$ transition.[16,72] Population of the $\frac{1}{2}^+$ level requires reevaluation of the 1028±15-keV Q value for ^{113}Sn decay.[73] These results form the basis for testing our unified description of the In nuclei.

II. EXPERIMENTAL PROCEDURE AND RESULTS

A. Source of 53.46-h ^{115}Cd^g

Sources of ^{115}Cd^g were made by the ^{114}Cd(n,γ) reaction in enriched ^{114}CdO targets at the Livermore pool type reactor (LPTR). Chemically pure, thin samples were isolated by standard radiochemical techniques.[74,75] These samples were then electroplated on Al counting disks. Spectral measurements were made with an absolutely calibrated low-energy photon spectrometer (LEPS) to give intensities as precise as possible from 10 to 300 keV. We used several large-volume Ge(Li) spectrometers to obtain the relative γ-ray intensities above 100 keV. Spectra were taken with up to 25.4 mm of Pb absorber to accentuate the γ rays with energies greater than 600 keV. An unseparated source was followed for approximately seven half-lives to assure that γ rays normally associated with ^{115}Cd^m had a ^{115}Cd^g component. The γ-ray energies were determined by counting ^{115}Cd^g sources simultaneously with known γ-ray energy standards on both LEPS and large-volume Ge(Li) systems. These techniques and their accuracy are discussed in Ref. 61. All spectra in this study were analyzed by the computer code GAMANAL developed by Gunnink and Niday.[62]

A separate experiment was performed to obtain Compton-suppression spectra. In this experiment, a first source of ^{115}Cd^g was produced by irradiating enriched ^{114}CdO in the LPTR center-core position for a day. The first source was removed and a new target placed in the LPTR for irradiation. The irradiated first source was then chemically purified and placed at the source position of a Compton-suppression spectrometer. Thus, each day we obtained a newly irradiated ^{115}Cd^g source and replaced the source from the previous day with it.

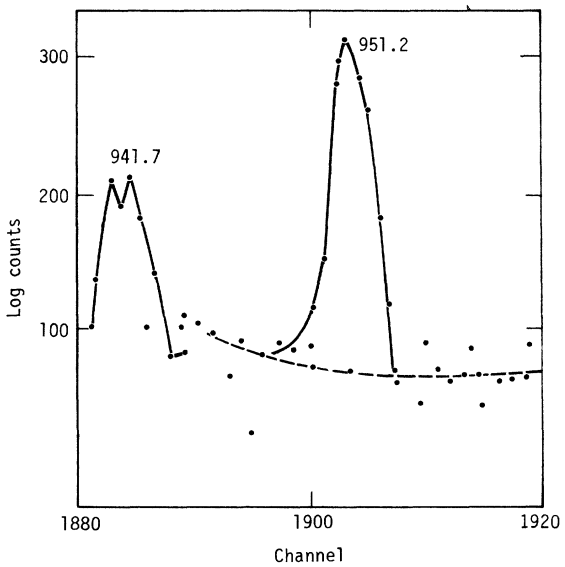

FIG. 1. Detail from Compton-suppression spectra showing the 941.7- and 951.2-keV photopeaks.

TABLE I. Energies and intensities of γ rays from decay of $^{115}Cd^{g}$.

E_γ (ΔE_γ) (keV)	I_γ (ΔI_γ)[a] (per 10^4 decays)	Assignment From	To
35.514 (3)	42.1 (3)	864	828
231.443 (3)	74 (1)	828	597
252 (1)	0.009 (7)	1193	1941
260.896 (3)	194 (1)	597	336
266.985 (10)	9.2 (3)	864	597
328.380 (95)	0.33 (5)	1192	828
336.301 (3)	4969[a] (22)	336	g.s.
363.950 (95)	0.61 (6)	1192	828
492.351 (4)	803 (9)	828	336
497.370 (29)	5.47 (8)	Sn 497	g.s.
527.901 (7)	2745 (18)	864	336
595.375 (24)	0.17 (2)	1192	597
690.227 (41)	0.061 (6)	1287	597
705.180 (250)	0.008 (2)	1042	336
856.245 (13)	0.22 (1)	1192	336
941.420 (11)	0.007 (1)	941	g.s.
951.187 (59)	0.028 (3)	1287	336
1078.2 (–)	<0.0002	1078	g.s.

[a]Transient equilibrium value; corrected value: 4602.

This was continued until approximately 150 h of counting time was obtained. The day-old sources were measured using Pb absorbers and large-volume Ge(Li) spectrometers. In Fig. 1 we show a detail from the Compton-suppression spectra that demonstrates the presence of the 941.7- and 951.2-keV γ rays. In Table I we present the γ-ray energies and intensities for decay of $^{115}Cd^{g}$.

B. Sources of 4.3-h $^{115}In^{m}$

An enriched ^{114}CdO target was irradiated for 5 days in the LPTR, removed, and allowed to decay after dissolution and the addition of In carrier. The indium was milked from the cadmium by precipitation of $In(OH)_3$ followed by a scavenger with CdS. The $^{115}In^{m}$ was mounted as In_2O_3 on an Al counting disk. A second milking was performed after a 3-day delay that allowed the $^{115}In^{m}$ to grow in. Singles Ge(Li) spectra were then taken with large-volume Ge(Li) spectrometers. A representative spectrum is shown in Fig. 2. For the 497.37-keV γ ray in the decay of 4.5-h $^{115}In^{m}$ we obtain a $0.025\pm0.001\%$ abundance, which is approximately $\frac{1}{3}$ the value originally reported.[54]

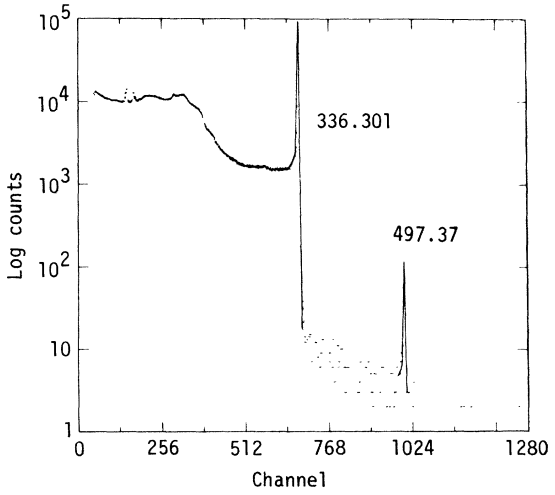

FIG. 2. Spectra of $^{115}In^{m}$ decay.

C. Sources of 44.6-day $^{115}Cd^{m}$

Thin sources of $^{115}Cd^{m}$ with a 10- to 20-μCi strength were prepared in a manner similar to that described in Sec. II A except that the irradiation period was 1 week and the delay was approximately 1 month. We counted these sources on LEPS and large-volume Ge(Li) spectrometers to obtain precise intensity values for the more abundant γ rays.[61] In addition we also used these sources to determine γ-ray energies of $^{115}Cd^{m}$ decay by simultaneous counting with a standard.[61]

We performed an initial Compton-suppression experiment with $^{115}Cd^{m}$ by first irradiating an enriched ^{114}CdO target for 2 months in the highest-flux position of the LPTR. After a 2 month delay to allow decay of the $^{115}Cd^{g}$, we chemically purified the $^{115}Cd^{m}$. The resulting source had a strength of approximately 200 mCi. The Compton-suppression spectrum of this source was taken for a period of approximately 1 month. This was followed by spectra taken with large-volume Ge(Li) spectrometers and Pb absorbers up to 25 mm thick. These latter spectra were significantly different than that reported by Sergeev *et al.*[9] In particular, the only γ-ray energies of Ref. 9 we could confirm were

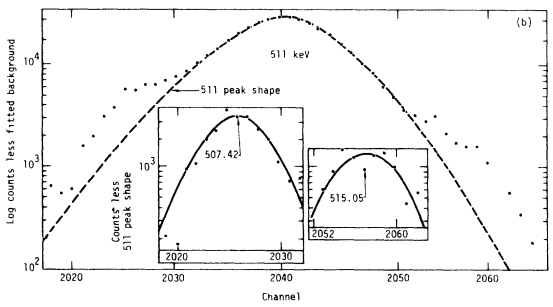

FIG. 3. Detailed area from the Compton-suppression spectrum of $^{115}Cd^{m}$ showing the 507-, 511-, and 515-keV photopeaks. (*Nota bene*: The plot is from the individual photopeak output routine of the GAMANAL computer-code analysis. The inserted spectra show the deviation of experimental counts from the 511 peak shape analysis.)

231 and 261 keV. Also, we could not observe some of the reported higher-energy γ rays because their intensity was low and the bremsstrahlung background was high.

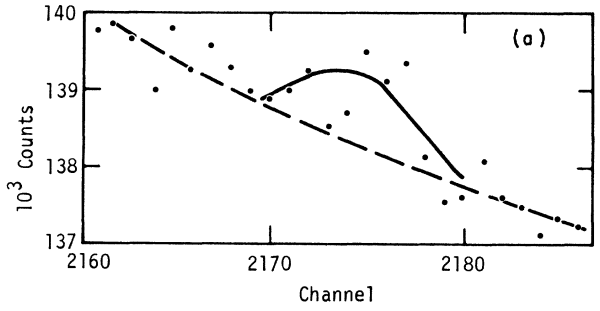

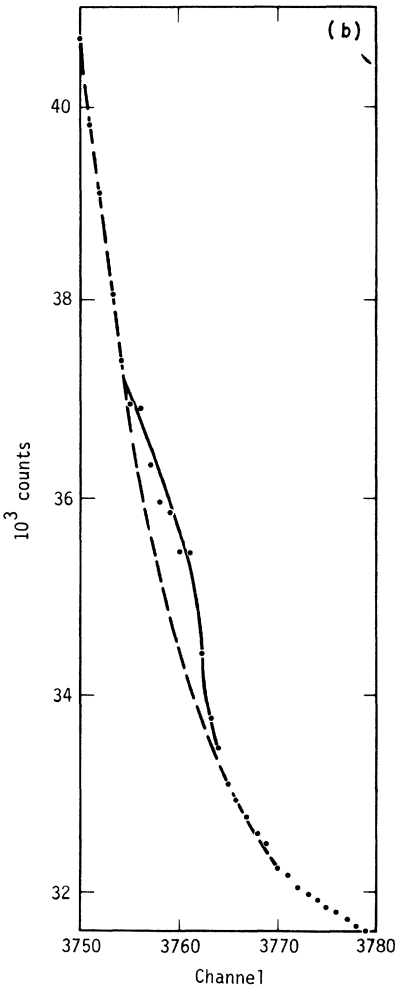

FIG. 4. Detailed areas from Compton-suppression spectra of $^{115}Cd^m$ showing (a) the 544.7-keV photopeak area and (b) the 933-keV photopeak.

A second Compton-suppression experiment was undertaken in which we produced a 2-Ci source of $^{115}Cd^m$ by irradiating a target of enriched ^{114}CdO at the Oak Ridge National Laboratory's high flux isotope reactor (HFIR).[76] Several spectra were taken from this source over a 6-month decay period. Two types of Compton-suppression measurements were performed: spectra taken without absorbers and with a gain of 0.25 keV per channel and spectra taken with an Al absorber and 12.5-mm Pb absorber. In the latter, the Al absorber significantly reduced the intense bremsstrahlung background while the Pb absorber significantly reduced summing. After the 6-month period, $^{110}Ag^m$ was the only impurity detectable in the $^{115}Cd^m$. The final spectrum was taken through the Pb absorber for a time long enough to gain satisfactory statistics in the high-energy $^{110}Ag^m$ lines. This spectrum was then used to energy-calibrate the high-energy $^{115}Cd^m$ γ rays for the presence of $^{110}Ag^m$.[61]

In Figs. 3 and 4 we show representative areas of the Compton-suppression spectra taken without absorbers. In Fig. 5 we show the Compton-suppression spectrum taken through the Pb absorber in the energy range from 1400 to 1520 keV. The insert shows the 1450- to 1520-keV energy range in an early spectrum. The results of all these measurements are given in Table II. We note that, as in the $^{115}Cd^g$ decay, our intensity results are different from those of earlier studies mainly because of increased knowledge of the Ge(Li) efficiency, as discussed in Ref. 61.

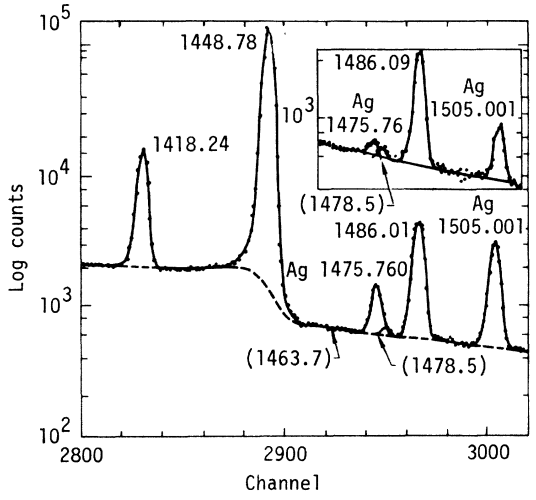

FIG. 5. Detail of $^{115}Cd^m$ Compton-suppression spectra taken through a 12.5-mm Pb absorber, showing the area from 1400 to 1520 keV. The insert shows the 1450- to 1520-keV area from spectra taken several months previous to spectra in the main figure.

TABLE II. Energy and intensity values for γ rays observed in the decay of $^{115}Cd^{m}$.

E_γ (ΔE_γ) (keV)	I_γ (ΔI_γ)[a] (relative)	Assignment From	Assignment To
105.200 (25)	2.21 (9)	933	828
158.027 (20)	8.51 (9)	1290	1132
231.440 (20)	0.44 (3)	828	597
260.890 (30)	0.46 (4)	597	336
316.201 (17)	1.24 (5)	1448	1132
336.301 (15)	2.47 (8)	336	g.s.
334.6 (1)	0.02 (1)	941	597
370.61 (7)	0.004 (2)	1448	1078
476.67 (15)	0.05 (1)	1418	941
484.471 (15)	145 (1)	1418	933
492.351 (5)	4.8 (1)	828	336
497.370 (29)	0.03 (2)	Sn 497	g.s.
507.361 (62)	0.13 (1)	1448	941
515.050 (70)	0.05 (2)	1448	933
544.7 (2)	0.043 (9) {0.03 / 0.01}[b]	{1478 / 1486}[b]	{933 / 941}[b]
933.838 (4)	1000 (3)	933	g.s.
941.680 (120)	0.12 (1)	941	g.s.
1078.2 (5)[c]	0.02 (2)[c]	1078	g.s.
1132.573 (11)	42.8 (5)	1132	g.s.
1290.585 (11)	445 (7)	1290	g.s.
1418.243 (11)	0.92 (4)	1418	g.s.
1448.776 (6)	8.5 (1)	1448	g.s.
(1463.7 (–))	(<0.000 05)	(1463)	(g.s.)
1478.5 (3)[d]	0.005 (3)	(1478)[d]	(g.s.)[d]
1486.099 (11)	0.28 (1)	1486	g.s.

[a] For absolute intensities, an error of 2% must be added in quadrature to account for the error in the knowledge of the efficiency curve.

[b] We apportion this intensity based on the relative values measured by Tuttle *et al.*[16] (see text).

[c] The relatively large error is due to the γ ray occurring in the spectra at approximately the same energy as the high-energy side of a Compton peak.

[d] We observe the 1478.5-keV γ ray in several of the Compton-suppression spectra taken through Pb absorbers. However, the spectra taken at later times exhibit interference from ^{110}Ag (see Fig. 5). Because our γ-ray data are the only evidence for this level, we take the assignment as tentative until confirmed by other experiments (see Sec. III, Decay Scheme and Level Assignment).

D. Sources of 115.1-d ^{113}Sn

To measure the relative intensity of the 646.75-keV crossover $E3$ γ ray that depopulated the second excited state of ^{113}In, we studied the decay of ^{113}Sn. Details of our original experiment are given in Refs. 63 and 64. Sources of up to 0.1 Ci were produced by the ^{112}Sn(n,γ) reaction on enriched ^{112}Sn. These sources were purified by ion-exchange techniques after a 3-month delay. This delay allowed any ^{125}Sb [produced by the ^{124}Sn(n,γ) reaction] and 9-day ^{125}Sn (produced by decay of ^{125}Sb) to decay to insignificant levels. Compton-suppression spectra were taken through Pb absorbers of thickness up to 25 mm which totally absorbed the 225- and 391-keV γ rays. The measurements were repeated three times over a period of 1 year, which is approximately three half-

TABLE III. Energy and intensity values of γ rays observed in the decay of ^{113}Sn.

E_γ (ΔE_γ) (keV)	I_γ (ΔI_γ) (relative)[a]	Assignment From	Assignment To
255.060 (50)	28.5 (7)	646	391
382.030 (–)	b	(1029)	(646)
391.688 (15)	1000(a)	391	g.s.
638.030 (75)	0.014 9 (5)	1029	391
646.8 (1)[c]	0.000 06 (3)[c]	646	g.s.

[a] For absolute γ-ray intensities, multiply by 6.49×10^{-4} (see Ref. 61 and add 2% error in quadrature to the intensity error [accounts for uncertainty of the Ge(Li) efficiency]).

[b] A limit of <0.001 can be set for the 1029- to 646-keV level transition.

[c] This value was obtained when 25 mm of lead was used as absorber during a Compton-suppression experiment. Therefore, no 255+391 summing was possible.

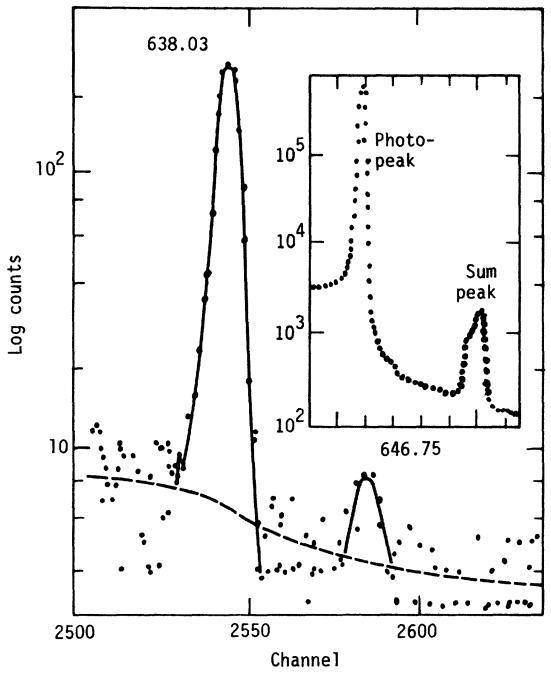

FIG. 6. Detail of ^{113}Sn Compton-suppression spectra taken through 25 mm of Pb absorber showing 638- and 646-keV photopeaks. For comparison, the insert shows a segment of ^{121}Te Compton-suppression spectrum taken on the same spectrometer. Note the difference in peak shape between the true photopeak on the left part of the insert and the sum peak on the right.

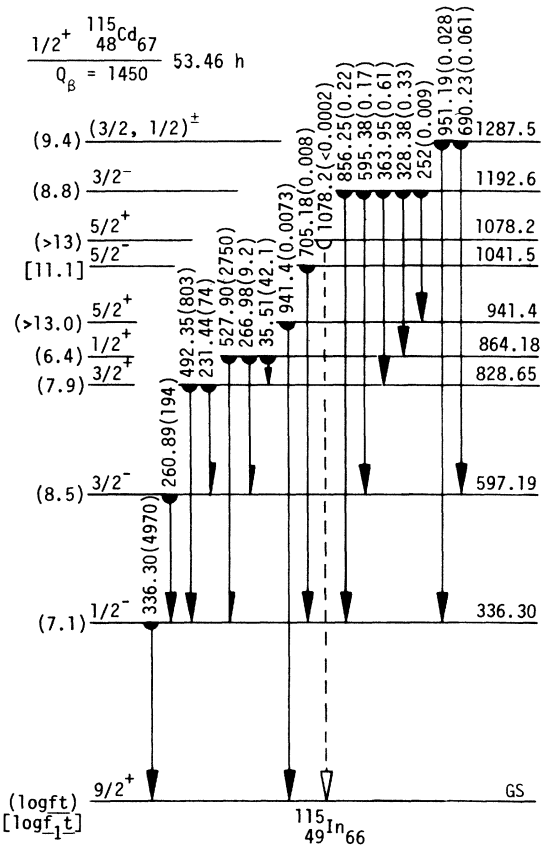

FIG. 7. Decay scheme for ^{115}Cd^{g}.

lives of the 115.1-day ^{113}Sn.[77] The results, including spectra taken on computer-controlled spectrometers that record channel overflow,[61] are given in Table III. In Fig. 6 we present a portion of a Compton-suppression spectrum taken through the Pb absorber. The spectrum shows the 638.03- and 646.75-keV photopeaks.

III. DECAY SCHEME AND LEVEL ASSIGNMENT

A. ^{115}Cd^{g} decay and ^{115}In levels

In Fig. 7 we present the ^{115}Cd^{g} decay scheme we deduce from our experimental results, previous studies,[41,65-68] and reaction spectroscopy studies.[78] As we noted earlier, our γ-ray intensities differ from previous values because the relative shape of the Ge(Li) efficiency response is now better known. Because of this, a more critical analysis can be made of the character of the excited levels.

We identify population of several levels in the decay of ^{115}Cd^{g} that have not previously been observed in its decay. These are the 941-, 1041-, 1192-, and 1287-keV levels. The 941-keV level has been observed in reaction spectroscopy studies[16] and Coulomb excitation studies.[7] It has been previously assigned a J^{π} of $\frac{5}{2}^{+}$. Our initial studies were the first to point out that the 1041-keV level was the hitherto unidentified $1f_{5/2}$ hole state in ^{115}In. The original arguments were based on the logft value, the identification of the 1041-keV level in $(d, {}^{3}\mathrm{He})$ transfer-reaction studies, and the absence of this level's excitation in Coulomb excitation studies.[7,78] This has since been confirmed by the level's strong excitation in (p,α) studies.[31] Neither the 1192- nor the 1287-keV level has been observed before. Their population by $\frac{1}{2}^{+}$ ^{115}Cd^{g}, their γ-ray branching, and the systematics of the odd-mass In nuclei suggest $\frac{3}{2}^{-}$ for the 1192- keV level and a $\frac{3}{2}^{-}$ or $\frac{1}{2}^{-}$ assignment for the 1287-keV level.

B. ^{115}Cd^{m} decay and ^{115}In levels

Although much work has been reported on the decay of ^{115}Cd^{m}, little additional information has been added since the study of Graeffe *et al.*[56] Recently Sergeev *et al.*[9] have suggested the presence of a number of additional lines of rather low intensity. Unfortunately, they show no spectra or photopeak areas to verify the quality of their data. As mentioned earlier, several of our initial experiments disagreed with the Sergeev *et al.*[9] study.

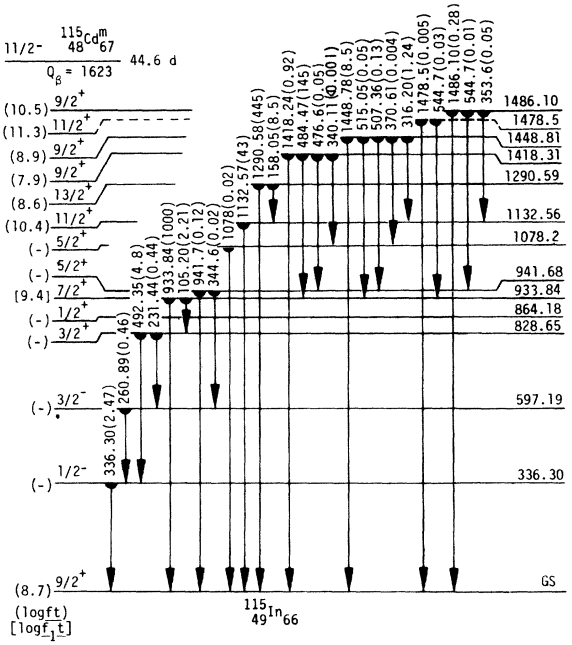

FIG. 8. Decay scheme for $^{115}Cd^{m}$.

The $^{115}Cd^{m}$ decay scheme that we deduce from our detailed studies is shown in Fig. 8.

Several new features of the $^{115}Cd^{m}$ decay and the ^{115}In levels this decay populates should be discussed. We find no evidence for either a 386- or 1463-keV γ ray as reported by Sergeev *et al.*,[9] and for these transitions we set intensity limits that are 20 and 2500 less, respectively, than they reported. Although our original Compton-suppression spectra did not show the 507- and 941-keV γ rays reported by Sergeev *et al.*,[9] we were able to identify both these transitions in the second Compton-suppression experiment. However, our intensities are lower than those reported in Ref. 9 (e.g., the 941-keV γ ray has $\frac{1}{4}$ the intensity suggested by Sergeev *et al.*). We do observe the 231- and 261-keV transitions. That these belong to the $^{115}Cd^{m}$ decay and not to the presence of $^{115}Cd^{g}$ fed by an isomeric transition is supported by our limit of approximately 0.0005 γ-ray units for the 527.90-keV γ ray, which is known to be the second most intense γ ray in $^{115}Cd^{g}$ decay.

We observe a 544-keV γ ray for the first time and find some evidence for a 1478-keV γ ray. These suggest a level at 1478.5 keV, as shown in Fig. 8. Such a level could have been overlooked in both transfer-reaction and Coulomb-excitation[72] studies because of the excitation in those studies of the 1448.8-, 1463.7-, and 1486.1-keV levels. A 544.7-keV γ ray is observed by Tuttle *et al.*[16] to depopulate the Coulomb excited 1486-keV level. The ratio of the intensities of the 544- and 1486-keV γ rays in their work is 3.7 to 78.7 (or 0.013 to 0.28, normalizing to our 1486-keV γ ray intensity). We conclude that our 544.7-keV peak is a doublet and calculate a 0.03 intensity for the transition between the 1478- and 933-keV levels (see Table II). Additionally, we note that in our studies of $^{117}Cd^{m}$ decay[75] we can identify an $\frac{11}{2}^{+}$ level at 1209.03 keV. This level feeds the 748.05-keV $\frac{7}{2}^{+}$ level 6 times greater than it decays to the ground state. In ^{115}In, the branching ratio we measure is about 6. We use this comparison to tentatively assign the 1478-keV level as the $\frac{11}{2}^{+}$ member of a band built on the 864-keV level.

The 1463-keV level observed in recent reaction spectroscopy studies[54] deserves mention. Sergeev *et al.*[9] suggested that this level has a J^{π} value of $\frac{7}{2}^{+}$ and Dietrich *et al.*[7] find the 1463-keV γ ray to be strongly Doppler-broadened, indicating that the transition is predominantly $M1$. Sergeev reported that this level is populated in $^{115}Cd^{m}$ decay with a logft of 10. Our data set a limit of logft > 13.5 which is unusually high for a unique first-forbidden transition.

We do observe the population of the 1078-keV $\frac{5}{2}^{+}$ level. However, it is fed entirely from decay of the 1418- and 1448-keV levels.

C. Decay of $^{115}In^{m}$ and levels of ^{115}Sn

The decay of $^{115}In^{m}$ is shown in Fig. 9. Using our γ-ray intensities, the total conversion coefficients,[79,80] and previous studies of ground-state β intensities,[78] we calculate 0.025% feeding to the 497.37-keV level of ^{115}Sn. This feeding value, the 4.3-h half-life of $^{115}In^{m}$, and the log$f$ values of Gove and Martin[81] yield a logft value of 7.5. This value is higher than previously reported, but is more consistent with the expected value for such a decay.[54]

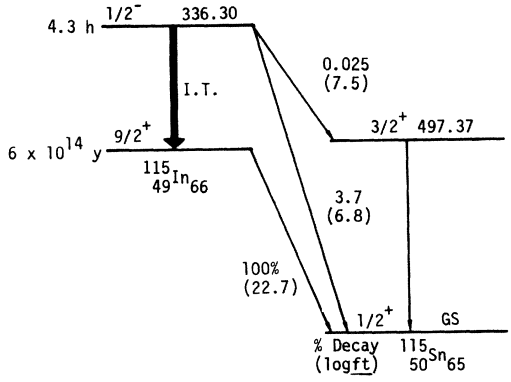

FIG. 9. Decay scheme for $^{115}In^{m}$.

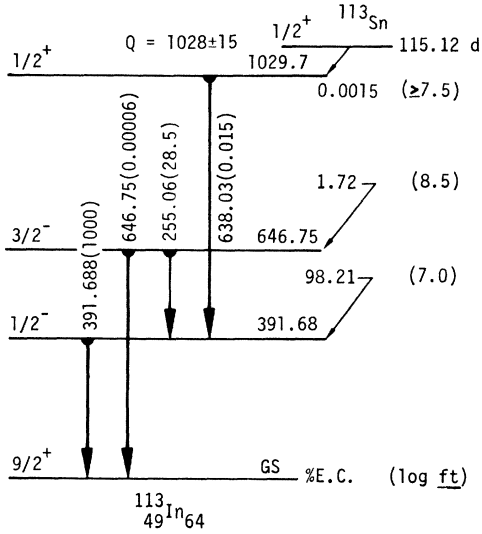

FIG. 10. Decay scheme for ^{113}Sn.

D. Decay of ^{113}Sn and levels of ^{113}In

The decay scheme for ^{113}Sn is shown in Fig. 10. Its half-life was recently measured as 115.12±0.20 days.[78] We place the 638-keV γ ray as representing the decay of a level at 1029.71 keV. This level, which we first proposed as being populated in β decay,[64] has been observed in the reaction spectroscopy studies of Markham and Fulbright.[70,71] Kim and Robinson,[17] in their (p,n) studies, measured the half-life of the 1029-keV level to be 0.33 ns. Because the decay energy has been measured as 1028±15 keV, the logft for β decay to the 1024-keV level can only be estimated. If we take the upper limit of 1043 keV for the correct value, the logft would be 7.5.

The 646-keV level decays to the 391.7-keV ($\frac{1}{2}^-$) level via an $M1+E2$ transition and to the ground state via an $E3$ transition. From Tuttle *et al.*'s[16] value for the $B(E3)$, our branching ratio of $I(646)/I(255)=2\times10^{-6}$, and the measured (Ref. 54) $E2/M1$ mixing ratio of $\delta^2=0.4$, one can calculate the $M1$ partial half-life. The ratio of this value to the Moszkowski estimate[78] is ≈8, an $M1$ hindrance factor that is comparable to those found[69,75] in other In nuclei for the transitions between the lowest-lying $\frac{3}{2}^-$ and $\frac{1}{2}^-$ states.

IV. UNIFIED DESCRIPTION OF THE ODD-MASS In ISOTOPES

In the calculations we perform, the configuration space of single-hole states coupled to the collective excitations of the Sn core is extended with all 1p-2h (seniority $v=1$ and $v=3$) states coupled to the same core. Therefore, the residual interactions between the 1p-2h configurations as well as between 1p-2h and 1h configurations will be important in determining the structure of the low-lying (0.5 MeV $< E_x <$ 1.5 MeV) positive-parity states in the odd-mass In isotopes.

A. Model Hamiltonian and two-step procedure

The Hamiltonian for the interacting system described above can be written as

$$H = E_0 + \sum_\lambda b_\lambda^\dagger b_\lambda [\hbar\omega_\lambda + \tfrac{1}{2}(2\lambda+1)] + \sum_\alpha \epsilon_a N(c_\alpha^\dagger c_\alpha) + \sum_{\alpha,\beta,\lambda,\mu} \langle\alpha|Y_{\lambda\mu}|\beta\rangle [b_{\lambda\mu}^\dagger + (-1)^\mu b_{\lambda-\mu}] N(c_\alpha^\dagger c_\beta) + \frac{1}{4}\sum_{\alpha,\beta,\gamma,\delta} V_{\alpha\beta\gamma\delta} N(c_\alpha^\dagger c_\beta^\dagger c_\delta c_\gamma), \quad (4.1)$$

in which E_0 denotes the total energy of the $I^\pi=0^+$ ground state in the doubly-even Sn nuclei and the normal product is defined with respect to this physical ground state, denoted by $|\tilde{0}\rangle$. The core-coupling term then takes into account the particle-hole and particle-hole-core coupling, whereas $V_{\alpha\beta\gamma\delta}$ describes the residual interaction between the proton single-particle degrees of freedom. If we put the restrictions on α, β, γ, and δ explicitly (according to the configuration space defined earlier), the Hamiltonian can be rewritten as

$$H = H_c + H_{\text{s p}} + H_{\text{s h}} + H_{\text{p core}} + H_{\text{h core}} + H_{\text{ph core}} + V_{\text{hh}} + V_{\text{ph}}, \quad (4.2)$$

where H_c describes low-lying collective excitations ($\lambda=2,3$) of the doubly-even core nucleus (Sn); $H_{\text{s p.}}$ and $H_{\text{s h.}}$, the proton single-particle and single-hole states, respectively; $H_{\text{p core}}$, $H_{\text{h core}}$, and $H_{\text{ph core}}$, the interaction of the single-hole, -particle, and -particle-hole motion with the surface vibrations of the core; and V_{hh} and V_{ph} the residual hole-hole and particle-hole interaction.

In a first step we diagonalize part of the Hamiltonian given in Eq. (4.1) [or Eq. (4.2)] to describe the low-lying levels ($E_x<2$ MeV) in the doubly-even Cd nuclei. We obtain the secular equation

$$\left(H_{\text{s.h}} + H_c + H_{\text{h core}} + V_{\text{hh}}\right)|\text{Cd};I^{(i)}M\rangle = \omega(I,i)|\text{Cd};I^{(i)}M\rangle, \quad (4.3)$$

where the Cd eigenstates are expanded as

$$|\text{Cd};I^{(i)}M\rangle \equiv \Omega_{I,i}^\dagger(\text{Cd})|\tilde{0}\rangle \equiv \sum_{h_1,h_2,J,R} d^{(i)}[(h_1h_2)J,R;I] \times[(\tilde{c}_{h_1}\tilde{c}_{h_2})_J \otimes \Omega_R^\dagger(\text{Sn})]_{IM}|\tilde{0}\rangle. \quad (4.4)$$

Here, R is a shorthand notation for $(N_o R_o, N_q R_q)R$, where N and R denote the number of phonons and the angular momentum, respectively. The labels o and q mean octupole or quadrupole type of vibrations.

The annihilation operator is defined as $c_{j_a,m_a} \equiv (-1)^{j_a+m_a} c_{j_a,-m_a}$. Calculations of this type have already been performed by Alaga *et al.*[26,27] to describe ^{114}Cd. Abecasis[5] makes the basic assumption that the low-lying levels in the doubly-even Cd nuclei have the same collective structure as those in the doubly-even Sn nuclei, except for a $(1g_{9/2}^{-2})_{0^+}$ two-hole configuration. This assumption is only fulfilled rather well for the $I^\pi = 0_1^+$ ground state (see Table I of Ref. 27). This can easily be verified by a calculation of the wave functions resulting from $I^\pi = 0_1^+$, $0_2^+, 2_1^+, 2_2^+$, and 4_1^+. We have redone this calculation with the parameters that we will discuss in Sec. IV B and obtain almost the same conclusions as in Ref. 27.

In a second step we consider the possibility of coupling proton configurations outside the $Z = 50$ closed shell to low-lying levels in the doubly-even Cd nuclei by constructing the configurations

$$[c_p^\dagger \otimes \Omega_{I,i}^\dagger(\mathrm{Cd})]_{JM}|\tilde{0}\rangle . \tag{4.5a}$$

Levels in the 2h-core coupled system up to an energy of 2 MeV are taken into account, which is almost equivalent with considering up to three quadrupole phonon states in ^{114}Cd for a phenomenological particle-core (Cd) coupling calculation (in ^{114}Cd we have $\hbar\omega_2 = 0.558$ MeV).

Also in the second step, we consider the hole-core (Sn) configurations

$$[\tilde{c}_h \otimes \Omega_R^\dagger(\mathrm{Sn})]_{JM}|\tilde{0}\rangle . \tag{4.5b}$$

The wave function describing excitations in the odd-mass In isotopes can then be taken to consist of hole-core (Sn) coupled states:

$$|j_h^{-1}, \mathrm{Sn}(R); JM\rangle \equiv [\tilde{c}_h \otimes \Omega_R^\dagger(\mathrm{Sn})]_{JM}|\tilde{0}\rangle , \tag{4.6}$$

and particle-core (Cd) coupled states:

$$|j_p, \mathrm{Cd}(I,i); JM\rangle \equiv [c_p^\dagger \otimes \Omega_{I,i}^\dagger(\mathrm{Cd})]_{JM}|\tilde{0}\rangle . \tag{4.7}$$

The wave function then results in

$$|J^\alpha M\rangle = \sum_{h,R} h^\alpha(hR;J)|j_h^{-1}, \mathrm{Sn}(R); JM\rangle + \sum_{p,I,i} p^\alpha(pIi;J)|j_p, \mathrm{Cd}(I,i); JM\rangle . \tag{4.8}$$

The secular equations for the odd-mass In nuclei, written in matrix form, become

$$\begin{bmatrix} H(hR,h'R';J) + \tilde{\epsilon}_h + \sum_\lambda \hbar\omega_\lambda N_\lambda & L(hR,p'I'i';J) \\ L(h'R',pIi;J) & K(pIi,p'I'i';J) + \omega(I,i) \end{bmatrix} \begin{bmatrix} h^\alpha(h'R';J) \\ p^\alpha(p'I'i';J) \end{bmatrix} = E(J^\alpha) \begin{bmatrix} h^\alpha(hR;J) \\ p^\alpha(pIi;J) \end{bmatrix} . \tag{4.9}$$

Notations of the H, L, and K matrix elements are given explicitly in Appendix A. The single-hole energies are denoted by $\tilde{\epsilon}_h$ $(\equiv -\epsilon_h)$, and N_λ gives the number of phonons of multipolarity λ.

The separate core-coupling calculations in the two subsystems now become coupled by means of the $(H_{\text{ph core}} + V_{\text{ph}})$ term in the Hamiltonian [Eq. (4.2)], whereas in the particle-core (Cd) coupled system the residual interaction V_{ph} will also modify the results of a more phenomenological particle-core coupling calculation, as performed by Abecasis.[5] If the assumption made by Abecasis is considered in calculating the K matrix element, one obtains the simplified result

$$K(pIi,p'i';J) = -4 \sum_J F(1g_{9/2}\, j_p\, 1g_{9/2}\, j_{p'};J) \frac{2J+1}{(2j_p+1)10} \delta_{II'}\delta_{j_p j_{p'}}\delta_{ii'} + \langle\tilde{0}|[c_p^\dagger \otimes \Omega_R^\dagger(\mathrm{Sn})]_{JM}|H_{\text{p core}}|[c_{p'}^\dagger \otimes \Omega_{R'}^\dagger(\mathrm{Sn})]_{JM}|\tilde{0}\rangle . \tag{4.10}$$

Here, the angular momentum I reduces to the core angular momentum R, as defined for the Sn core. However, only quadrupole vibrations are considered.

If a pairing force is used as residual interaction, the contributions from V_{ph} become zero, and the resulting contributions from other forces (δ force, etc.) remain small compared with the $H_{\text{p core}}$ con-

tribution. The coupling strength expressed as

$$\xi_2\hbar\omega_2 = \left\langle r\,\frac{\partial V}{\partial r}\right\rangle \frac{4(5\pi)^{1/2}}{3ZeR_0^{\,2}} B(E2;2_1^+\to 0_1^+)^{1/2}$$

is used,[28] along with

$$B(E2;2_1^+\to 0_1^+)^{1/2}_{^{114}\mathrm{Cd}} / B(E2;2_1^+\to 0_1^+)^{1/2}_{^{116}\mathrm{Sn}} = 1.4\,.$$

(Ref. 29) for application in ^{115}In. Although the $H_{\text{p core}}$ term is still defined with respect to the Sn core, the coupling strength $(\xi_2\hbar\omega_2)_{\mathrm{Sn}}$ is nearly equal to $(\xi_2\hbar\omega_2)_{\mathrm{Cd}}$, and the second term of Eq. (4.10) can then be reinterpreted as the result of a particle-core coupling calculation where all collective operators are defined in the Cd nucleus. In our actual calculations (applied to ^{115}In), the deviations caused by admixtures other than $(1g_{9/2}^{-2})_{0^+}$ and by the presence of a non-negligible residual interaction V_{ph} tend to renormalize the particle-coupling strength $(\xi_2\hbar\omega_2)_{^{116}\mathrm{Sn}}$ toward the value to be considered in an empirical particle-core (Cd) calculation, where $(\xi_2\hbar\omega_2)_{^{114}\mathrm{Cd}}$ is taken directly from the value of $B(E2;2_1^+\to 0_1^+)$ in ^{114}Cd.[29]

If one uses the simplifying assumption of Abecasis *et al.*,[5] the matrix element $L(h'R',pIi;J)$ connecting both subsystems reduces to

$$L(h'R',pIi;J) = -\left(\frac{2}{2j_{h'}+1}\right)^{1/2} |G(j_h j_h j_p j_{h'};0)\,\delta_{RR'} + (-1)^{j_p+J+R'} \times \begin{Bmatrix} j_{h'} & R' & J \\ R & j_p & 2 \end{Bmatrix} \langle j_h||Y_2||j_p\rangle (\xi_2\hbar\omega_2)_{\mathrm{Sn}} \langle R||b_2+b_2^\dagger||R'\rangle \delta_{j_h j_{h'}}|\,, \tag{4.11}$$

with $j_h \equiv 1g_{9/2}$. The residual interaction V_{ph} cannot connect both subsystems in the configuration space as chosen here ($1\hbar\omega$ excitation only), so that only $H_{\text{ph core}}$ gives nonvanishing matrix elements for Eq. (4.11).

B. Parameters

In our calculations, we have concentrated mainly on ^{115}In, because we could perform the most precise measurements on it and because this nucleus has the most complete set of documented ancillary measurements of all the In isotopes. Three different kinds of parameters occur: single-particle and single-hole energies, coupling strength, and the residual interaction $V_{\alpha\beta\gamma\delta}$. The $1g_{9/2}^{-1}$, $2p_{3/2}^{-1}$, $2p_{1/2}^{-1}$, and $1f_{5/2}^{-1}$ single-hole orbitals are taken into account and the $1g_{9/2}^{-1}$ orbital is taken as a reference level. We have determined the values of $\tilde\epsilon_{2p_{3/2}}$, $\tilde\epsilon_{2p_{1/2}}$, and $\tilde\epsilon_{2f_{5/2}}$ to describe the excitation energy and the spectroscopic factors in the reaction ^{116}Sn$(d,\tau)^{115}$In (Refs. 30–32) as well as possible for the $J^\pi = \frac{1}{2}^-_1$, $\frac{3}{2}^-_1$, and $\frac{5}{2}^-_1$ levels.

The energy for configurations in which a proton is excited through the $Z = 50$ closed shell is determined by $\epsilon_{1g_{7/2}} + \tilde\epsilon_{1g_{9/2}} + \omega(0_1^+, {}^{114}\mathrm{Cd})$ and can be taken from the Wapstra and Gove mass tables[33] to be $S_p(Z=51,N) - S_p(Z=49,N)$, yielding a value of 2.4 MeV in ^{115}In and 2.34 MeV in ^{117}In for the lowest 1p-2h configuration. The relative energies (relative to $1g_{7/2}$) for the other single-particle configurations ($2d_{3/2}$, $3s_{1/2}$, $1h_{11/2}$) are taken from the work of Reehal and Sorensen,[34] whereas the value of $\epsilon_{2d_{5/2}} - \epsilon_{1g_{7/2}}$ is taken as a parameter to fix the relative position of the lowest $J^\pi = \frac{1}{2}^+$ and $\frac{3}{2}^+$ states. Then, we use the following single-particle and single-hole energies (relative to $1g_{9/2}$ and $1g_{7/2}$, respectively):

$$\tilde\epsilon_{2p_{1/2}} = 0.60 \text{ MeV}, \quad \epsilon_{2d_{5/2}} = 0.50 \text{ MeV},$$
$$\tilde\epsilon_{2p_{3/2}} = 1.30 \text{ MeV}, \quad \epsilon_{2d_{3/2}} = 2.60 \text{ MeV},$$
$$\tilde\epsilon_{2f_{5/2}} = 2.00 \text{ MeV}, \quad \epsilon_{3s_{1/2}} = 2.95 \text{ MeV},$$
$$\epsilon_{1h_{11/2}} = 2.10 \text{ MeV}.$$

The coupling strengths ξ_2 and ξ_3 are taken from $B(E2;2_1^+\to 0_1^+)$ and $B(E3;3_1^-\to 0_1^+)$ values,[29,35] and the phonon energies $\hbar\omega_2$ and $\hbar\omega_3$ are taken from the excitation energies for the $I^\pi = 2_1^+$ and 3_1^- levels in ^{116}Sn. This gives as a result $\xi_2 = 2.5$ and $\xi_3 = 1.0$ (rounded-off values). Here one observes that the product $(\xi_2\hbar\omega_2)_{^{116}\mathrm{Sn}} = 3.20$ does not differ very much from the value of $(\xi_2\hbar\omega_2)_{^{114}\mathrm{Cd}} = 4.40$. In the ^{115}In calculation, up to three quadrupole phonon and two octupole phonon vibrations are taken into account, whereas in the ^{114}Cd nucleus, all levels with energies below 2 MeV have been considered. This energy cutoff corresponds roughly to a calculation for three quadrupole phonons and two octupole phonons in the more phenomenological particle-core (Cd) calculations. Unperturbed configurations [Eqs. (4.6) and (4.7)] up to 8.0 MeV are used to screen out truncation effects below $E_x \approx 2.5$ MeV in the final ^{115}In nucleus.

We have introduced the same force for both com-

ponents of the residual proton hole-hole as well as particle-hole interactions. By considering a δ force, one is able to explain the pairing properties in the two-hole configurations and still have non-negligible particle-hole matrix elements. As residual interaction, we then consider $V = V_0 \cdot \delta(\vec{r}_1 - \vec{r}_2)$ with $V_0 = -120$ MeV fm^3 (where V_0 was fixed by the requirement for a good description of the low-lying levels in ^{114}Cd within the unified-model calculation[26,27]).

V. THEORETICAL RESULTS

A. Energy spectrum

In Fig. 11, the unified-model calculated energy spectrum is compared with our experimental data. Both negative- and positive-parity states have been calculated. One can clearly observe the good agreement for the single-hole states as well as for the $|1g_{9/2}^{-1}, \mathrm{Sn}(2_1^+); J^\pi\rangle$ quadrupole vibrational multiplet. The rotational-like sequence of positive-parity states ($J^\pi = \frac{1}{2}^+, \frac{3}{2}^+, \ldots$) is also reproduced and mainly results from: (i) single-particle excitation through the $Z = 50$ closed proton shell for

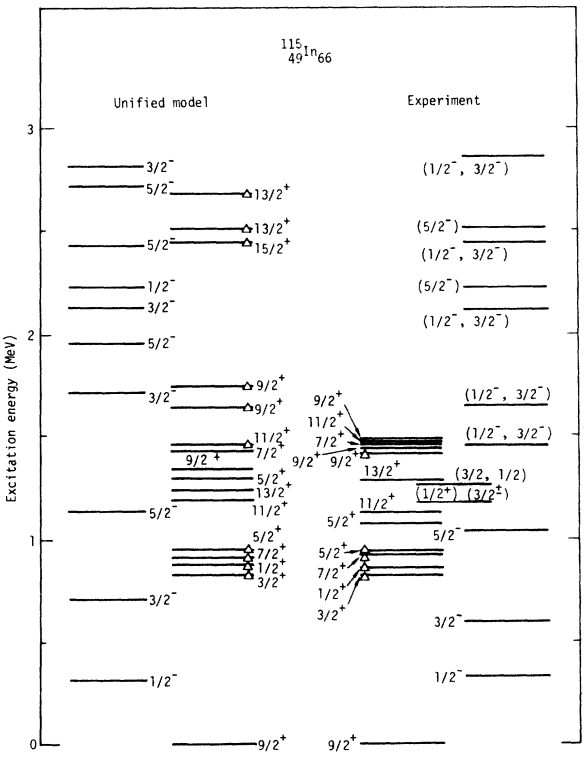

FIG. 11. The negative- and positive-parity levels calculated in a unified model are compared with the experimental data. Levels marked with a small triangle mainly consist of particle-core (Cd) coupled configurations.

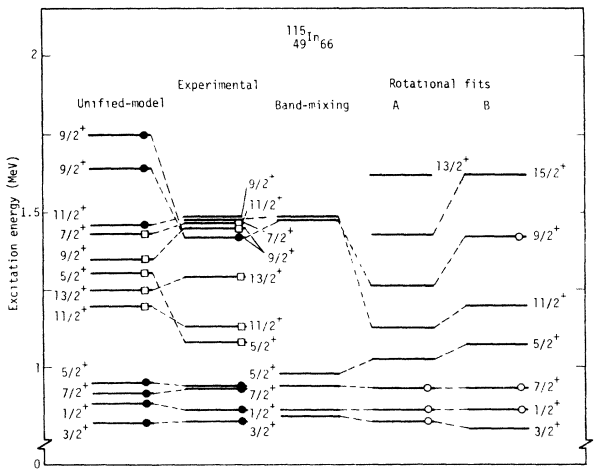

FIG. 12. Comparison of the positive-parity levels with the unified-model calculation, purely rotational $\Omega = \frac{1}{2}^+$ [431] fits (columns A and B) with different constraints on the fit levels (indicated with open circle), and the results of a band-mixing calculation. Open squares indicate the vibrational multiplet; filled circles show the rotational-like sequence of levels.

the corresponding angular momentum J^π, and (ii) large admixtures of the $|2d_{5/2}, \mathrm{Cd}(2_1^+); J^\pi\rangle$ and $|1g_{7/2}, \mathrm{Cd}(2_1^+) J^\pi\rangle$ configurations.

Also in the theoretical calculation, three $J^\pi = \frac{9}{2}^+$ levels occur at about 1.5 MeV. The lowest of these is the $|1g_{9/2}^{-1}, \mathrm{Sn}(2_1^+); \frac{9}{2}^+\rangle$ multiplet configuration, whereas the levels at 1.64 and 1.75 MeV are mainly built from the $|2d_{5/2}, \mathrm{Cd}(2_1^+); \frac{9}{2}^+\rangle$ and $|1g_{7/2}, \mathrm{Cd}(2_1^+); \frac{9}{2}^+\rangle$ configurations. Only small mixing between the hole-core (Sn) and particle-core (Cd) subsystems occurs as is evidenced by the γ-ray branching from the level we observe (see Fig. 8).

In Fig. 12, we compare the experimental positive-parity states in the energy region between 0.7 and 1.75 MeV with two different fits of a rotational band built on the $\frac{1}{2}^+[431]$ Nilsson orbital, a result from band-mixing calculations with all $N = 4$ harmonic-oscillator Nilsson orbitals (see Sec. VI), and with the result of the unified-model calculations. Only our calculation is able to explain both the vibrational multiplet and the rotational-like sequence. However, if we consider only the latter, then the band-mixing calculation gives the best description. Thus, concerning the energy spectrum, it is possible through the combined effect of both the residual particle-hole interaction V_{ph} and the particle-core (Cd) coupling ($H_{\mathrm{p\ core}} + H_{\mathrm{ph\ core}}$) to lower the relevant states $J^\pi = \frac{1}{2}^+, \frac{3}{2}^+, \ldots$ from their unperturbed position in the energy region between 2.4 and 3.0 MeV to the experimentally observed energy of about 1.0 MeV.

B. Spectroscopic factors

The single-particle and single-hole components of the calculated wave functions can undergo a first test in the calculation of the spectroscopic factors for (τ,d), (α,t),[22-24] and $(d,\tau)(p,t)$[25,30-32] reaction studies. The expressions are for proton pickup

$$S^{(\alpha)}_{l,j}(J) = h^{\alpha}(lj, 0^+_1; J)^2 \delta_{jJ} \; ; \tag{5.1}$$

for proton stripping to a single-particle state above $Z = 50$:

$$S^{(\alpha)}_{l,j}(J) = p^{\alpha}(lj, 0^+_1; J)^2 \delta_{jJ} \; ; \tag{5.2}$$

and for stripping into a level below $Z = 50$:

$$S^{(\alpha)}_{l,j}(J) = \Big| \sum_{h_1, h_2, h', R} h^{\alpha}(h'R; J)\, d^{(1)}[(h_1 h_2)R, R; 0](2J+1)^{-1/2} \times [\delta_{h_1 J}\delta_{h_2 h'} - (-1)^{J+j_{h'}-R}\delta_{h_2 J}\delta_{h_1 h'}](1+\delta_{h_1 h_2})^{-1/2}\Big|^2 . \tag{5.3}$$

However, if one uses the assumption of Abecasis[5] concerning the relation of collective vibrational states in ^{116}Sn and ^{114}Cd, Eq. (5.3) reduces to

$$S^{(\alpha)}_{l,j}(J) = \frac{2}{2J+1} h^{\alpha}(lj, 0^+_1; J)^2 \delta_{jJ} \; . \tag{5.4}$$

In Figs. 13 and 14, spectroscopic factors calculated according to Eqs. (5.1) through (5.3) are compared with the experimental data.[22-25,30-32] For the pickup reaction (Fig. 13), the calculated values are as good as earlier theoretical results.[1-3,5,6,30] Above $E_x = 1.5$ MeV, experimentally as well as theoretically, only small spectroscopic values result for $l = 1$ and $l = 3$ transfer. However, in the stripping-reaction studies (Fig. 14), the values for single-particle configurations above the $Z = 50$ core, such as $1g_{7/2}, 2d_{5/2}$, etc., agree well overall while the absolute values are too small by a factor of 2. Using the simple Nilsson-model interpretation for the rotational band built on top of the $\frac{1}{2}^+[431]$ intrinsic orbital, the spectroscopic factors are expressed as

$$S^{(\alpha)}_{l,j}(J) = \frac{2}{2J+1} c_{lj}{}^2 (\tfrac{1}{2}^+[431])\, \delta_{jJ} . \tag{5.5}$$

The expansion coefficients c_{lj} for the Nilsson wave functions have been calculated for the $\frac{1}{2}^+[431]$ orbital corresponding to the equilibrium deformation

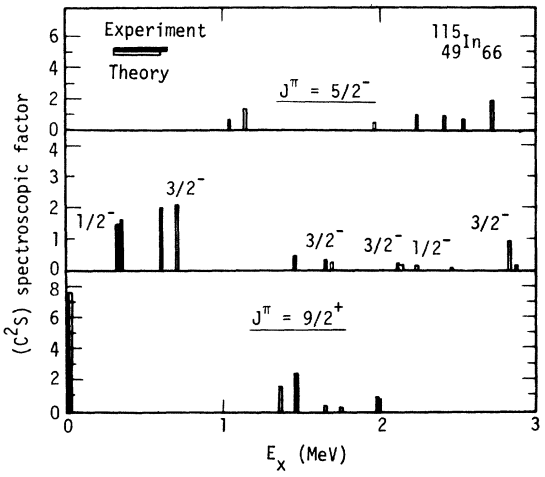

FIG. 13. Experimental spectroscopic factors from pickup reaction studies compared with those calculated from the unified model.

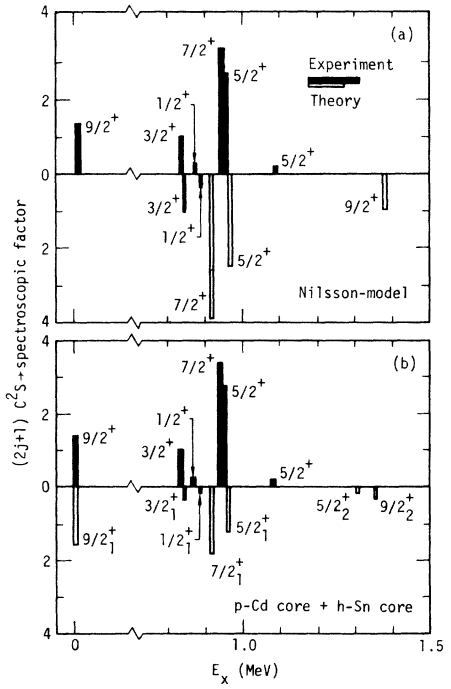

FIG. 14. Experimental spectroscopic factors from stripping reactions compared with (a) results obtained for a purely rotational band on top of the $\frac{1}{2}^+$ [431] Nilsson orbit and (b) those of unified-model calculations.

as obtained in the total potential energy (TPE) curves for ^{115}In,[36,42] and the results are indicated in Fig. 14(a). Results for spectroscopic factors as obtained from the band-mixing calculation (see Sec. VII A) do not differ significantly from the pure $\frac{1}{2}^+[431]$ rotational-band calculation.

In comparing the results shown in Figs. 14(a) and 14(b), we observe already a strong resemblance between the rotational description and the unified-model description in terms of 1p-2h excitations coupled to the quadrupole and octupole vibrations of the Sn core.

C. Static moments

Further understanding of the wave functions for ^{115}In can be obtained by calculating static moments (μ and Q) and electromagnetic transition rates ($E1$, $E2$, $E3$, and $M1$). In this section we discuss the static moments and in the next section we discuss the reduced transition probabilities. For this part of the calculation, some new quantities enter, such as the effective proton charge $e_p^{\rm eff}$, which is taken throughout as $1.5e$. For the gyromagnetic ratio we use $g_R = Z/A$, and we consider $g_s = 0.5 g_s^{\rm free}$ as the quenched proton intrinsic-spin value in the nucleus.

After straightforward but tedious calculations, the formulas for the static moments and transition rates are obtained. For a more detailed discussion see Appendix B. The operators we consider for the unified-model calculations[28] are for the electric operator:

$$M(E\lambda,\mu) = B(E\lambda;\lambda \to 0_1^+)_{\rm Sn}^{1/2}[b_{\lambda\mu}^\dagger + (-1)^\mu b_{\lambda-\mu}] + \sum_{\alpha,\beta} \langle\alpha| r^\lambda Y_{\lambda\mu} |\beta\rangle c_\alpha^\dagger c_\beta , \tag{5.6}$$

whereas the magnetic dipole operator is

$$M(M1,\mu) = g_R R_\mu + \sum_{\alpha,\beta} \langle\alpha| g_l l_\mu + g_s s_\mu |\beta\rangle c_\alpha^\dagger c_\beta . \tag{5.7}$$

Here again R denotes the total collective angular momentum in the core nucleus Sn, and $R_\mu \equiv R_{q,\mu} + R_{o,\mu}$.

The expression for the reduced matrix element between the initial state $|J_i^{(\alpha)} M_i\rangle$ and the final state $|J_f^{(\beta)} M_f\rangle$ is given in Appendix B. This rather complex expression (B1) can be separated (approximately) into:

(i) single-particle transitions in either the hole-core (Sn) subsystem or the particle-core (Cd) subsystem;
(ii) collective transitions in both subsystems;
(iii) single-particle transitions connecting the hole-core (Sn) and particle-core (Cd) subsystems (dominant for $E1$ transitions).

When one uses the assumption of Abecasis[5] concerning the relation between collective vibrational states in ^{116}Sn and ^{114}Cd, the reduced transition probability for the collective part of the $M1$ operator reduces [$(Z/A)^{116}{\rm Cd} \cong (Z/A)^{114}{\rm Sn}$, to a very good approximation] to the result of an empirical particle-core (Cd) coupling calculation [see Eq. (B2), Appendix B].

The static moments μ and Q are calculated with the parameters given above and are shown in Table IV. Here, we observe a rather good agreement with the scarce amount of experimental results.[20,21,37-40] The sequence of negative quadrupole moments for $J^\pi = \frac{1}{2}^+_1$, $\frac{3}{2}^+_1$, $\frac{5}{2}^+_1$, $\frac{7}{2}^+_1$, $\frac{9}{2}^+_{3,4}$, $\frac{11}{2}^+_2$, and $\frac{13}{2}^+_2$ levels will be discussed later. This sequence is a reflection of the single-particle character for which the proton is moving outside the $Z = 50$ closed shell. If, however, the calculated laboratory quadrupole moment for the $J^\pi = \frac{3}{2}^+_1$ level is transformed into an

TABLE IV. The magnetic dipole and electric quadrupole moments as calculated in a unified model for ^{115}In. Comparison with the experimental data is made.

	μ (μ_N)		Q (e b)	
J_α^π	Theory	Experimental	Theory	Experimental
$\frac{3}{2}^+_1$	0.687	0.80 ± 0.14 [a]	−0.615	|0.60 ± 0.08| [a]
$\frac{5}{2}^+_1$	3.696		−0.579	
$\frac{5}{2}^+_2$	3.704		0.148	
$\frac{7}{2}^+_1$	2.357		−1.132	
$\frac{7}{2}^+_2$	4.697		0.344	
$\frac{9}{2}^+_1$	5.880	5.336 [b,c]	0.685	|0.830| [d]
$\frac{9}{2}^+_2$	5.561		0.125	
$\frac{9}{2}^+_3$	4.131		−0.504	
$\frac{9}{2}^+_4$	6.259		−0.463	
$\frac{11}{2}^+_1$	6.570		0.490	
$\frac{11}{2}^+_2$	4.108		−0.981	
$\frac{13}{2}^+_1$	7.613		0.625	
$\frac{13}{2}^+_2$	6.233		−0.287	
$\frac{1}{2}^-_1$	−0.018			
$\frac{3}{2}^+_1$	4.007		0.299	

[a] Reference 38.
[b] Reference 40.
[c] Reference 21.
[d] Reference 39.

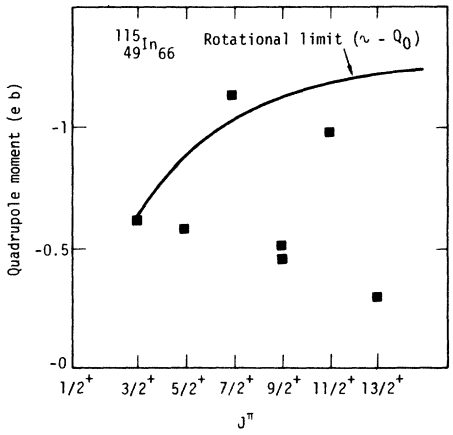

FIG. 15. Quadrupole moments for positive-parity levels $J^\pi = \frac{1}{2}^+_1, \frac{3}{2}^+_1, \cdots$ calculated in a unified model are compared with the purely rotational-model prediction for a $\frac{1}{2}^+$ [431] Nilsson orbital as bandhead.

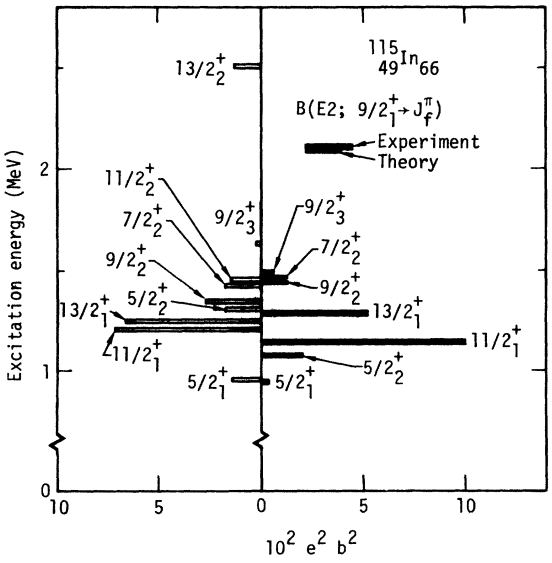

FIG. 16. Experimental Coulomb excitation $B(E2^+_1 \rightarrow J^+_f)$ values compared with unified-model calculated values.

intrinsic quadrupole moment, assuming $K = \frac{1}{2}$, a value of $Q_0(K = \frac{1}{2}) = 3.075\ e$ b results. This is very close to the experimental value of $3.0 \pm 0.4\ e$ b.[15,21] In Fig. 15, the pure rotational limit with this value of Q_0 is compared with the quadrupole moment calculated in the unified-model description of ^{115}In. Except for the $J^\pi = \frac{9}{2}^+_{3,4}$ (configuration mixing) and $\frac{13}{2}^+_2$ (truncation effects in the configuration space for high spins) levels, the rotational limit is rather well reproduced in a semimicroscopic approach.

D. Reduced transition probabilities

First we discuss the Coulomb excitation results and then we discuss the transitions inside the rotationlike sequence of positive-parity levels. In Table V we present the important wave function components in the positive-parity rotationlike sequence of levels. The theoretical $B(E2; \frac{9}{2}^+_1 \rightarrow J^\pi)$ values are shown in Fig. 16 and compared with the experimental results.[16-19] The overall agreement is again good because only the $|1g_{9/2}^{-1}\mathrm{Sn}(2^+_1); J^\pi\rangle$ multiplet is strongly excited. The theoretical mixing between $J^\pi = \frac{5}{2}^+_{1,2}$ levels however, is stronger than experimental data indicate.

The theoretical mixing between the vibrational $J^\pi = \frac{9}{2}^+_2$ and the $\frac{9}{2}^+_{3,4}$ levels is weaker than shown by existing data. Coulomb excitation of the other rotational-like members ($J^\pi = \frac{7}{2}^+_1, \frac{9}{2}^+_{3,4}, \frac{11}{2}^+_2$, and $\frac{13}{2}^+_2$) is very small and indicates the near coexistence of both hole-core (Sn) and particle-core (Cd) coupled states in ^{115}In.

If we now calculate the $B(E2)$ values inside the rotational-like sequence of levels, together with $B(E2)$ values for transitions connecting the rotational-like states with the $|1g_{9/2}^{-1}, \mathrm{Sn}(2^+_1); J^\pi\rangle$ multiplet, the scheme in Fig. 17 results. Here

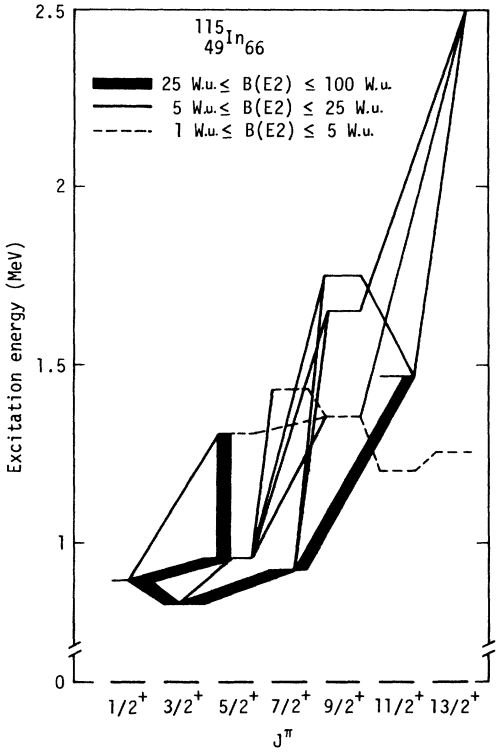

FIG. 17. The reduced $E2$ transition probabilities for transitions inside the rotational-like sequence of positive-parity levels, inside the vibrational multiplet $|1g_{9/2}^{-1}\mathrm{Sn}(2^+_1); J^\pi\rangle$, and connecting both subsystems. The intensity scale, indicated in the figure, is expressed in Weisskopf single-particle $E2$ units.

TABLE V. The most important components from the wave functions describing the positive-parity rotational-like sequence of levels, as calculated in a unified-model for ^{115}In (columns B). Also given (columns A) are the strong-coupling wave functions decomposed in the representation of Eq. (6.4), Sec. VI. For the $J^\pi = \frac{9^+}{2}_{3,4}$ and $\frac{13^+}{2}_{2,3}$ levels, the lower component is based on the ordering in excitation energy as obtained in the unified-model calculation.

$J^\pi = \frac{1}{2}^+_1$	A	B	$J^\pi = \frac{3}{2}^+_1$	A	B
$3s_{1/2}$	−0.40	−0.26	$2d_{3/2}$	0.37	0.28
$2d_{5/2}$, Cd(2^+_1)	−0.58	−0.48	$1g_{7/2}$, Cd(2^+_1)	0.62	0.50
$2d_{3/2}$, Cd(2^+_1)	+0.35	0.35	$2d_{5/2}$, Cd(2^+_1)	−0.19	−0.18
$1g_{7/2}$, Cd(4^+_1)	+0.30	0.44	$2d_{3/2}$, Cd(2^+_1)	−0.25	−0.25
			$3s_{1/2}$, Cd(2^+_1)	0.24	0.20
			$1g_{7/2}$, Cd(4^+_1)	−0.21	−0.26
			$2d_{5/2}$, Cd(4^+_1)	0.20	0.26

$J^\pi = \frac{5}{2}^+_1$	A	B	$J^\pi = \frac{7}{2}^+_1$	A	B
$2d_{5/2}$	−0.54	−0.44	$1g_{7/2}$	0.60	0.47
$1g_{7/2}$, Cd(2^+_1)	0.16	0.18	$1g_{7/2}$, Cd(2^+_1)	−0.46	−0.50
$2d_{5/2}$, Cd(2^+_1)	0.40	0.37	$2d_{5/2}$, Cd(2^+_1)	0.11	0.13
$2d_{3/2}$, Cd(2^+_1)	−0.17	−0.15	$2d_{3/2}$, Cd(2^+_1)	0.35	0.29
$3s_{1/2}$, Cd(2^+_1)	−0.35	−0.22	$1g_{7/2}$, Cd(4^+_1)	0.21	0.29
$1g_{7/2}$, Cd(4^+_1)	−0.16	−0.22	$2d_{5/2}$, Cd(4^+_1)	−0.10	−0.15
$2d_{5/2}$, Cd(4^+_1)	−0.17	−0.16	$2d_{3/2}$, Cd(4^+_1)	−0.12	−0.14
$2d_{3/2}$, Cd(4^+_1)	0.20	0.19	$3s_{1/2}$, Cd(4^+_1)	0.13	0.14

$J^\pi = \frac{9}{2}^+_{3,4}$	A	B	A	B	$J^\pi = \frac{11}{2}^+_2$	A	B
$1g_{7/2}$, Cd(2^+_1)	−0.12	0.31	−0.57	−0.49	$1g_{7/2}$, Cd(2^+_1)	0.73	0.62
$2d_{5/2}$, Cd(2^+_1)	−0.55	−0.50	0.16	−0.23	$1g_{7/2}$, Cd(4^+_1)	−0.36	−0.47
$1g_{7/2}$, Cd(4^+_1)	0.15	−0.14	0.56	0.48	$2d_{5/2}$, Cd(4^+_1)	0.10	0.15
$2d_{5/2}$, Cd(4^+_1)	0.27	0.40	−0.24	0.06	$2d_{3/2}$, Cd(4^+_1)	0.33	0.33
$2d_{3/2}$, Cd(4^+_1)	−0.16	−0.05	−0.21	−0.20	$1g_{7/2}$, Cd(6^+_1)	0.13	0.23
$3s_{1/2}$, Cd(4^+_1)	−0.28	−0.24	0.13	−0.10			
$2d_{5/2}$, Cd(6^+_1)	−0.09	−0.20	0.19	0.09			
$1g_{7/2}$, Cd(6^+_1)			−0.28	−0.25			

$J^\pi = \frac{13}{2}^+_{2,3}$	A	B	A	B
$1g_{7/2}$, Cd(4^+_1)	0.17	0.58	0.68	0.53
$2d_{5/2}$, Cd(4^+_1)	0.64	0.32	−0.21	−0.40
$1g_{7/2}$, Cd(6^+_1)	−0.15	−0.41	−0.48	−0.29
$2d_{5/2}$, Cd(6^+_1)	−0.25	−0.07	0.23	0.30
$2d_{3/2}$, Cd(6^+_1)	0.17	0.18	0.19	0.06
$3s_{1/2}$, Cd(6^+_1)	0.29	0.11	−0.12	−0.13

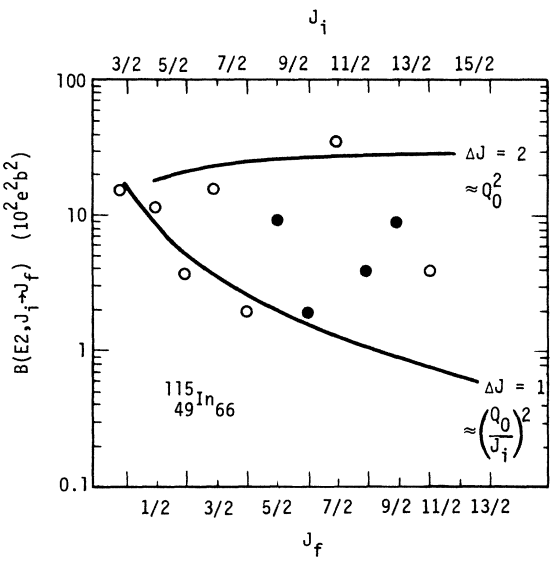

FIG. 18. The $\Delta J=2$ ($E2$) and $\Delta J=1$ ($E2$) reduced transition probabilities for the rotational-like sequence of positive-parity levels, as calculated in the unified model. Filled circles indicate transitions with the $J^\pi = \frac{9}{2}^+_4$ level occurring as the initial (J_i) or final (J_f) state. Curves give the purely rotational results for a $\frac{1}{2}^+$ [431] band. Asymptotic values in this case are also given.

the $B(E2)$ values are drawn schematically and clearly establish the rotational behavior of strong $\Delta J=2$ $E2$ transitions and small $\Delta J=1$ $E2$ transitions. In this figure, one also observes the fact that $B(E2)$ values inside the vibrational multiplet are of the order 1 W.u. $< B(E2) <$ 5 W.u. [for comparison $B(E2; 2_1^+ \to 0_1^+)$ for ^{114}Cd is 31 W.u.]. The transitions from the vibrational multiplet towards the rotational-like levels are small compared with the very strong $B(E2)$ values inside the rotational-like sequence.

In Fig. 18 our theoretical results are compared with results obtained in a pure rotational model, and again the intensity rules for $\Delta J=2$ and $\Delta J=1$ $E2$ transitions are well reproduced within our unified model. This alternation in the reduced $E2$ transition rates can be explained qualitatively in the unified-model description. There one observes, for the main components in the wave function for the $J^\pi = \frac{1}{2}^+_1, \frac{3}{2}^+_1, \ldots$ levels (see Table V, columns B), configurations dominated by the $2d_{5/2}$ and $1g_{7/2}$ single-particle states. We assume, for simplicity, a harmonic quadrupole spectrum for describing the low-lying ($E_x < 2$ MeV) levels in ^{114}Cd and obtain a zero-order description of levels in ^{115}In. In this description, one observes two bands developing:

(i) $J^\pi = \frac{1}{2}^+, \frac{5}{2}^+, \frac{9}{2}^+$, and $\frac{13}{2}^+$ with a $2d_{5/2}$ proton single-particle excitation coupled to the $I^\pi = 0_1^+, 2_1^+, 4_1^+$ collective quadrupole states,

(ii) $J^\pi = \frac{3}{2}^+, \frac{7}{2}^+$, and $\frac{11}{2}^+$ with a $1g_{7/2}$ proton single-particle excitation coupled to the $I^\pi = 0_1^+, 2_1^+, 4_1^+$ collective quadrupole states, where maximal alignment between the single-particle and collective angular momenta occurs (the $J^\pi = \frac{1}{2}^+$ and $\frac{3}{2}^+$ levels result from maximal antialignment).

In this description, strong $E2$ transitions only occur within the bands separately, because the collective part of the $E2$ operator contributes to $\Delta J = 2$ ($E2$) transitions with

$$B(E2; J_i \to J_f) = \frac{2}{2J_i+1} |\langle j, (N-1)_q R'_{q,\max}; J_f| \times \|M(E2; \text{coll})\| j, N_q R_{q,\max}; J_i\rangle|^2 = N_q B(E2; 2_1^+ \to 0_1^+). \quad (5.8)$$

(Here the reduced $E2$ transition probability is taken from ^{114}Cd.) For $E2$ transitions with $\Delta J = 1$, however, a change between bands is necessary, and only the single-particle part of the operator can contribute, resulting in a value of

$$B(E2; J_i \to J'_f) = \frac{1}{2J_i+1} |\langle j', N_q R_{q,\max}; J'_f| \times \|M(E2; \text{s.p.})\| j, N_q R_{q,\max}; J_i\rangle|^2. \quad (5.9)$$

Admixtures in both initial and final states, and ^{114}Cd not behaving as an harmonic quadrupole vibrator, modify this simple picture somewhat. The basic features as discussed above remain and dominate the $\Delta J = 2$ and $\Delta J = 1$ $E2$ transition rates between the rotational-like sequence of positive-parity states in ^{115}In. The intensity rules for $\Delta J = 2$ and $\Delta J = 1$ $E2$ transitions in a purely rotational model originate from the Clebsch-Gordan coefficient, giving as a result

$$B(E2; J_i \to J_f) = \frac{5}{16\pi} Q_0^2(\tfrac{1}{2}^+[431]) |C^{1/2\ 0\ 1/2}_{J_i\ 2\ J_f}|^2. \quad (5.10)$$

This expression for J_i and J_f tending to infinity shows the asymptotic intensity pattern

$$B(E2; J_i \to J_f) = \frac{5}{16\pi} Q_0^2(\tfrac{1}{2}^+[431]) \tfrac{3}{8} (\Delta J = 2), \quad (5.11)$$

$$B(E2; J_i \to J_f) = \frac{5}{16\pi} Q_0^2(\tfrac{1}{2}^+[431]) \frac{3}{8J_i^2} (\Delta J = 1). \quad (5.12)$$

(Already for relatively small values of J_i, J_f ($\frac{3}{2}, \frac{5}{2}$), the asymptotic values are approached within 15%.) Thus, for $\Delta J = 2$ and $\Delta J = 1$ in ^{115}In, we can give a qualitative explanation for the strong resemblance between those $B(E2)$ values calcu-

lated in a unified-model approach and those resulting from a purely rotational band structure on top of the $\frac{1}{2}^+[431]$ intrinsic orbital [see Eqs. (5.8) through (5.12)].

In the $^{111\text{-}119}$In isotopes, highly retarded $E1$ transitions have been observed,[13,15] connecting the $J^\pi = \frac{1}{2}^+_1, \frac{3}{2}^+_1$ levels with the $J^\pi = \frac{1}{2}^-_1, \frac{3}{2}^-_1$ levels. In the unified model, highly hindered (compared with the Weisskopf estimate) reduced $E1$ transition rates result but are still too high, compared with the experimental data. The $E1$ matrix element results from single-particle transitions connecting particle-core (Cd) and hole-core (Sn) configurations. Here, the $3s_{1/2}$, $2d_{3/2}$, $2d_{5/2}$, and/or $1g_{7/2}$ proton single-particle orbits are considered, resulting in the occurrence of the $2p_{1/2}$, $2p_{3/2}$, and $1f_{5/2}$ proton single-hole orbits [see the second term in Eq. (B1) in Appendix B]. The only configurations that can contribute are those where the two-hole cluster, describing $I^\pi = 0^+_1$ and 2^+_1 levels in ^{114}Cd, consists of either $(2p_{1/2}{}^{-2})_{0^+}$, $(2p_{3/2}{}^{-2})_{0^+}$, and/or $(2f_{5/2}{}^{-2})_{0^+}$. These configurations occur with small amplitude (see Table I of Ref. 27), so the resulting $E1$ reduced transition probability will be highly retarded. The results of these considerations are indicated in Table VI, from which one observes a discrepancy still of two orders of magnitude.

The observation of $E3$ deexcitation and $E3$ Coulomb excitation for the $J^\pi = \frac{3}{2}^-_1$ level is reproduced rather well in the unified model, indicating nonnegligible octupole phonon components in the wave function for this level. The calculation yields $B(E3; \frac{9}{2}^+_1 \to \frac{3}{2}^-_1) = 7.02 \times 10^{-75}\ e^2\,\mathrm{cm}^6$ [experiment gives $5.73 \pm 0.35 \times 10^{-75}\ e^2\,\mathrm{cm}^6$ (Ref. 16)]. This value results from constructive interference between the single-hole $1g_{9/2}{}^{-1} \to 2p_{3/2}{}^{-1}$ transition and the collective $1g_{9/2}{}^{-1} \to |\, 1g_{9/2}{}^{-1}, \mathrm{Sn}(3^-_1); \frac{3}{2}^-_1\rangle$ (amplitude-0.334) $E3$ transitions; these transitions have nearly equal amplitude.

Finally, in Table VII, the known $M1$ transitions in ^{115}In are compared with the experimental data[16] and with other calculations.[2,3,5] Here, we clearly observe good agreement of the unified model with experiment and also a general overall agreement with the results of Abecasis.[5]

TABLE VI. The hindrance factor, expressed in Weisskopf units, for the strongly retarded $E1$ transitions in ^{115}In.

$J^\pi_i \to J^\pi_f$	$E1$ hindrance factor Theory	Experiment[a]
$\frac{1}{2}^+_1 \to \frac{1}{2}^-_1$	6.1×10^3	7.4×10^5
$\to \frac{3}{2}^-_1$	5.9×10^4	4.3×10^7
$\frac{3}{2}^+_1 \to \frac{1}{2}^-_1$	1.6×10^2	2.5×10^6
$\to \frac{3}{2}^-_1$	6.3×10^4	3.2×10^6

[a] Reference 15.

TABLE VII. Comparison of unified-model with experimental and other theoretical $B(M1)$ values for ^{115}In.

$J^\pi_i \to J^\pi_f$	$B(M1) \times 10^2$ $(\mu_N)^2$ Experimental[b]	Theory[a] A	B	C	D
$\frac{11}{2}^+_1 \to \frac{9}{2}^+_1$	30^{+53}_{-15}	18	21	15.9	13.8
$\frac{13}{2}^+_1 \to \frac{11}{2}^+_1$	64 ± 4	39	30	30.2	45.1
$\frac{9}{2}^+_2 \to \frac{9}{2}^+_1$	$0.03^{+2.7}_{-0.03}$		2	1.7	0.70
$\frac{9}{2}^+_2 \to \frac{11}{2}^+_1$	37^{+50}_{-12}	66	35	37.5	54.8
$\frac{7}{2}^+_2 \to \frac{9}{2}^+_1$	20^{+60}_{-16}	25	26	18.2	19.1
$\frac{7}{2}^+_1 \to \frac{9}{2}^+_1$	0.5 ± 0.3				5.5
$\frac{7}{2}^+_2 \to \frac{5}{2}^+_2$	70^{+193}_{-55}	58	42	30.5	11.4
$\frac{9}{2}^+_3 \to \frac{9}{2}^+_1$	3^{+12}_{-2}			0.8	1.8
$\frac{9}{2}^+_3 \to \frac{11}{2}^+_1$	26^{+236}_{-20}				24.7

[a] A, Ref. 2; B, Ref. 3; C, Ref. 5; D, this work.
[b] Reference 16.

E. Comparison with other calculations

We have demonstrated that the unified-model calculations performed for ^{115}In can account for almost all phenomena observed without resorting to extra, deformed states (such as the rotational band on top of the $\frac{1}{2}^+[431]$ orbital). The older calculations of Covello[3] and Iachello[6] do not even attempt to explain an important part of the ^{115}In energy spectrum. Sen[2] and Mang[4] introduce deformed states in a purely empirical way. The calculation of Abecasis[5] comes close in idea to our unified-model calculation, although one of his basic assumptions for connecting the collective vibrational states in ^{114}Cd and ^{116}Sn is not fulfilled very well, as shown in a calculation of the ^{114}Cd level scheme and wave functions up to $E_x < 2$ MeV.[26,27] However, the differences between the final results of his theory and ours are small. This is because:

(i) Extra configurations other than

$$[(\tilde{c}_{1g_{9/2}}\tilde{c}_{1g_{9/2}})_0 \otimes \Omega^\dagger_R(\mathrm{Sn})]_{\mathrm{IM}}\,|\,\tilde{0}\rangle$$

are important in describing the $I^\pi = 0^+_1$, 0^+_2, 2^+_1, 2^+_2, and 4^+_1 levels in ^{114}Cd.

(ii) Particle-hole (V_{ph}) interactions contributes significantly to the calculation of matrix elements

for the particle-core (Cd) configurations.

Both (i) and (ii) act to renormalize the coupling strength $(\xi_2\hbar\omega_2)_{^{116}\mathrm{Sn}}$, here and in the subsystem for particle-core (Cd) coupled configurations [see Eq. (4.10)], tending to increase toward the coupling strength of $(\xi_2\hbar\omega_2)_{^{114}\mathrm{Cd}}$ as taken from the $B(E2;2_1^+ \rightarrow 0_1^+)$ value in ^{114}Cd. Although our calculation contradicts one of the basic assumptions of Abecasis,[5] the final results concerning energy spectra differ little. Larger differences occur in the electromagnetic transition rates.

VI. CALCULATIONS IN A DEFORMED BASIS

The origin of the low-lying positive-parity "intruder" states has been suggested to be the $\frac{1}{2}^+[431]$ Nilsson orbital.[8,41] However, it was not until recently that detailed calculations of the TPE surfaces for odd-mass In isotopes were performed.[36,42] In these, one clearly observes a well pronounced deformed minimum with $0.10 < \epsilon_2 < 0.20$ for $^{107\text{-}119}$In, corresponding to the $\frac{1}{2}^+[431]$ Nilsson orbital. The excitation energy, defined as the difference between the deformed minimum and the "odd-even" background for a spherical shape, ranges from 1.0 to 1.6 MeV.[36] [The "odd-even" background is identified with the total energy calculated when the quasiparticle energy $E_{1qp}(\Omega,i)$ equals Δ, i.e., the smallest energy possible in the odd-mass nucleus.] Similar calculations have been performed by Ragnarsson (see for example Ref. 42) where also the parameters of the Nilsson model[43] ($\kappa_{p,n}$, $\mu_{p,n}$, and pairing strength $G_{p,n}$) are extensively discussed. For the $\frac{1}{2}^+[431]$ Nilsson state considered going from $\epsilon_2 = 0.15$ to $\epsilon_2 = 0.20$, the decoupling parameter a only changes from 0.22 to −0.42. These small values completely disagree with the fitted values of $a = -2.0$, -2.20 (see A and B, respectively, in Fig. 12) for a description of ^{115}In.

A. Band-mixing calculation

We have performed a complete band-mixing calculation[44-46] for ^{115}In as well as for the other $^{107\text{-}119}$In isotopes. We have then taken into account all Nilsson orbitals originating from the $N=4$ harmonic-oscillator shell and performed the calculation at the equilibrium deformation of the $\frac{1}{2}^+[431]$ orbital. Strong mixing with the nearby $\frac{1}{2}^+[420]$ and $\frac{3}{2}^+[422]$ orbitals is expected to modify the rotational-band structure considerably and is the most probable explanation for the anomalous decoupling parameter a used to fit the rotational-like sequence. The strong-coupling wave functions[28] $|JM;\Omega i\rangle$ can be expanded in a basis where the core angular momentum is a good quantum number:

$$|jJ_c;JM\rangle = \sum_m C^{m\ M-m\ M}_{j\ J_c\ J} \left(\frac{2J_c+1}{8\pi^2}\right)^{1/2} D^{M-m,0}_{J_c}(\omega)^* \alpha^\dagger_{j,m} |\phi(\mathrm{core})\rangle , \tag{6.1}$$

where ω denotes the Euler angles and $\alpha^\dagger_{j,m}$ creates a quasiparticle in the orbital with quantum numbers (n,l,j,m). The interaction matrix element for the core and single-particle Hamiltonian[28] then results in

$$\langle JM;\Omega i|H_{\mathrm{core}}+H_{\mathrm{s.p.}}|JM;\Omega' i'\rangle = 2\sum_{j,J_c} (-1)^{j-\Omega} C^{\Omega\ -\Omega\ 0}_{j\ J\ J_c} (-1)^{j-\Omega'} C^{\Omega'\ -\Omega'\ 0}_{j\ J\ J_c} \cdot E_{j_c} \cdot c_j(\Omega',i')\, c_j(\Omega,i)$$
$$\times (u_{\Omega,i}u_{\Omega',i'} + v_{\Omega,i}v_{\Omega',i'}) + E_{1qp}(\Omega,i)\delta_{\Omega\Omega'}\delta_{ii'} . \tag{6.2}$$

Here, E_{J_c} describes the core energy $[\hbar^2/2J \cdot J_c(J_c+1)$ in a rotational nucleus, one can verify that, for $E_{J_c} = \hbar^2/2J \cdot J_c(J_c+1)$, the normal Coriolis coupling and decoupling matrix elements result], $c_j(\Omega,i)$ the Nilsson expansion coefficient, $v^2_{\Omega,i}$ the occupation probability, and $E_{1qp}(\Omega,i)$ the corresponding quasiparticle energy. In our calculations, the experimental excitation energies in the underlying doubly-even Cd nuclei have been taken[47,48] as core energies (up to $J_c^\pi = 12^+$ to describe states in the odd-mass In isotopes up to $J^\pi = \frac{15}{2}^+$). Whenever the higher-spin states are not observed experimentally, we extrapolate toward $J_c^\pi = 12^+$. We have studied the sensitivity of the level schemes in the odd-mass In isotopes by varying the extrapolated Cd core energies $(J_c^\pi = 8^+, 10^+, 12^+)$; only small changes result. The final wave function at the energy $E(J^\alpha)$ is obtained as

$$|J^\alpha M\rangle = \sum_{\Omega,i} d^\alpha(\Omega i, J) |JM;\Omega i\rangle , \tag{6.3}$$

B. Parameters and results

Before discussing the results, we remark that from ^{107}In to ^{119}In the change in $1g_{7/2}$ proton single-

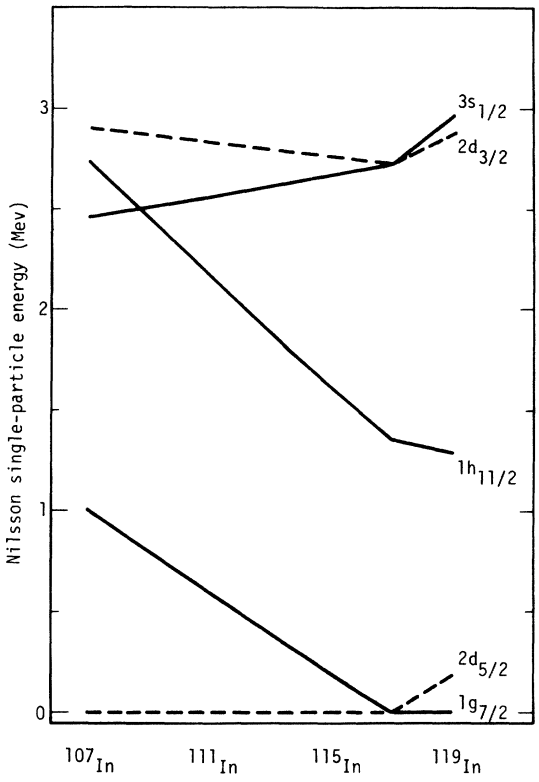

FIG. 19. Variation of Nilsson single-particle energies (at $\epsilon_2 = 0$) with increasing neutron number, $^{107-119}$In. This variation is caused by varying $\mu_P = 0.375$ (^{107}In) to $\mu_p = 0.525$ (^{119}In) in steps of 0.025.

particle energy (relative to $2d_{5/2}$) will influence the detailed structure of the Nilsson wave functions considerably. Therefore, and because we intend to describe the finer details of the positive-parity rotational-like sequence $J^\pi = \frac{1}{2}^+_1, \frac{3}{2}^+_1, \ldots$, we must consider the variation of $\Delta_\epsilon \equiv \epsilon_{1g_{7/2}} - \epsilon_{2d_{5/2}}$ from ^{107}In to ^{119}In. (This variation of Δ_ϵ is not very important in calculating global properties of the nucleus such as TPE and the subsequent equilibrium deformation corresponding with the $\frac{1}{2}^+[431]$ orbital.) We can account for the change in Δ_ϵ by varying μ_p from 0.375 (^{107}In) to 0.525 (^{119}In) in steps of 0.025. The resulting change in the calculated single-particle energy (for $\epsilon_2 = 0$) is shown in Fig. 19. The change in Δ_ϵ corresponds very well to the analogous change in Δ_ϵ for the Sb isotopes.[49-51]

The resulting energy spectra are shown in Fig. 20, relative to the $J^\pi = \frac{1}{2}^+_1$ level. Here, one observes that band mixing is very important in determining the precise ordering and energy separation for the different members of the rotational-like sequence. For $^{107-113}$In however, problems occur with respect to the position of the $J^\pi = \frac{5}{2}^+_1$ level. There is some mixing with the nearby $|1g_{9/2}^{-1}\mathrm{Sn}(2^+_1); \frac{5}{2}^+\rangle$ configuration that cannot be reproduced in the present calculation in a deformed basis. The calculation indicates that it is probably the lowest experimental $J^\pi = \frac{5}{2}^+$ level which occurs as a member of the rotational band (as in ^{107,109}In). The wave functions for the J^π levels between $\frac{1}{2}^+$ and $\frac{15}{2}^+$ in ^{115}In are shown in Table VIII. Here one ob-

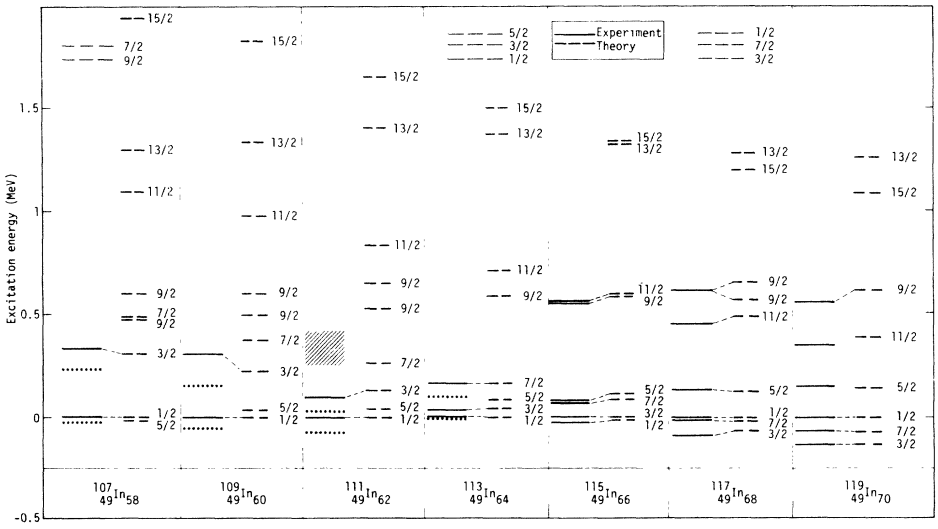

FIG. 20. Results from band-mixing calculation (full $N = 4$ harmonic-oscillator shell) compared with experimental positive-parity, rotational-like levels in $^{107-119}$In. Calculation is normalized to the energy position for the $J^\pi = \frac{1}{2}^+$ level. Dotted line indicates possible fragmentation for the $J^\pi = \frac{5}{2}^+$ levels; hatched region indicates the expected position for the $J^\pi = \frac{7}{2}^+$ level.

TABLE VIII. Expansion coefficients $d^{\alpha}(\Omega i;J)$ [see Eq. (6.3)], resulting from a band-mixing calculation for the rotational band mainly built on the $\frac{1}{2}^+[431]$ Nilsson orbital.

J^{π}	$\frac{1}{2}^+[431]$	$\frac{1}{2}^+[420]$	$\frac{3}{2}^+[422]$	$\frac{3}{2}^+[411]$	$\frac{5}{2}^+[422]$	$\frac{5}{2}^+[413]$	$\frac{7}{2}^+[413]$	$\frac{9}{2}^+[404]$
$\frac{1}{2}^+$	0.95	−0.29						
$\frac{3}{2}^+$	0.94	0.21	0.25					
$\frac{5}{2}^+$	0.85	−0.43	0.27	−0.14				
$\frac{7}{2}^+$	0.80	0.41	0.41			0.12		
$\frac{9}{2}^+$	0.76	−0.42	0.30	−0.16	0.17		0.22	−0.19
$\frac{11}{2}^+$	0.76	0.45	0.43	0.11		0.13		
$\frac{13}{2}^+$	0.77	−0.43	0.32	−0.17	0.12			−0.17
$\frac{15}{2}^+$	0.74	0.47	0.43	0.13		0.15		

serves the growing importance of the $\frac{1}{2}^+[420]$ and $\frac{3}{2}^+[422]$ Nilsson orbitals with increasing angular momentum. We can conclude that, although at lower spin values ($J^{\pi} \leq \frac{5}{2}^+$) the sequence of states very well resembles a pure $\frac{1}{2}^+[431]$ rotational band, at the higher angular momenta a decoupled band structure built on, respectively, the $2d_{5/2}$ and $1g_{7/2}$ single-particle orbits develops (see also Sec. V D). By transforming the final wave functions to the basis (6.1), we obtain[44-46]

$$|J^{\alpha}M\rangle = \sum_{j,J_c,m,M_c} C^{m\,M_c\,M}_{j\,J_c} [U_{jJ_c}(J^{\alpha})c^{\dagger}_{j,m} + V_{jJ_c}(J^{\alpha})\tilde{c}_{j,m}]|J_cM_c\rangle . \tag{6.4}$$

Here $|J_cM_c\rangle$ describes the core states of the doubly-even Cd nuclei, and the expansion coefficients are given by

$$U_{jJ_c}(J^{\alpha}) = \sum_{\Omega,i} \left[\frac{2(2J_c+1)}{2J+1}\right]^{1/2} C^{\Omega\ 0\ \Omega}_{j\ J_c\ J} c_j(\Omega,i) d^{\alpha}(\Omega i;J) u_{\Omega,i} , \tag{6.5}$$

and a similar expression for $V_{jJ_c}(J^{\alpha})$.

Comparing the wave functions $|J^{\alpha}M\rangle$ for $J^{\pi} = \frac{1}{2}^+$ through $\frac{15}{2}^+$ (Table V, columns A) with the results from the unified-model calculation for ^{115}In reveals (i) The suggested decoupled band structure for the higher-spin members of the $\frac{1}{2}^+[431]$ rotational-like sequence becomes very clear, and the $2d_{5/2}$ and $1g_{7/2}$ single-particle orbits are mainly involved. (ii) The same structure results from the unified-model approach (Table V, columns B). For the $J^{\pi} = \frac{13}{2}^+$ levels, however, the important components occur in a reversed order compared with those of the deformed calculation.

As pointed out (see Sec. V E), truncation effects can already play a role for the description of high-angular-momentum states in the unified-model description.

In the unified-model calculation, admixtures in the wave functions $|J^{\alpha}M\rangle$ when a single-particle component with angular momentum J exists are such that configurations $|j, \mathrm{Cd}(2_1^+); J\rangle$ with $j = J$ or $J \pm 2$ have large amplitudes whereas $j = J \pm 1$ admixtures have small amplitudes. First-order perturbation theory can explain this alternation: The reduced matrix element $\langle J||Y_2||j\rangle$ determines the amplitude for the configurations given above.[52] The asymptotic ($j, J \to \infty$) selection rules[52] for the reduced matrix element immediately explain the strong alteration in amplitude shown in Table V, columns B.

VII. CONCLUSION

We have shown that if one takes into account the coupling of both single-hole and 1p-2h excitations (seniority $v = 1$ and $v = 3$) to the quadrupole and octupole vibrations of the underlying core nucleus, a rich variety of nuclear phenomena result. In our calculations, both the vibrational multiplet $|1g_{9/2}^{-1}\mathrm{Sn}(2_1^+J); J^{\pi}\rangle$ and the rotational-like sequence $J^{\pi} = \frac{1}{2}_1^+, \frac{3}{2}_1^+, \ldots$ of positive-parity states at low excitation energy ($E_x \approx 1.0$ MeV) result and are seen to interact only weakly. One exception is the $J^{\pi} = \frac{5}{2}^+$ levels, where moderate mixing occurs. In the

calculation of spectroscopic factors for the ^{114}Cd (^{3}He, d)^{115}In reaction our results are similar to those from a Nilsson-model calculation, in which the positive-parity levels result from a rotational band on top of the $\frac{1}{2}^+[431]$ orbital. The unified model is able to explain, by means of the 1p-2h excitations, the more phenomenological approach, where proton single-particle excitations through the $Z = 50$ closed shell are coupled to the vibrational excitations of the Cd core nucleus. The negative quadrupole moments for the rotational-like sequence of levels are also reproduced in the unified-model approach. The reduced $E2$ transition probabilities $B(E2)$ inside this rotational-like sequence strongly suggest a purely rotational explanation.

To better understand the equivalence between the rotational model and calculations starting from either spherical single-particle orbits and quadrupole vibrations or single-hole orbits and octupole vibrations of the underlying core nucleus, we have performed a band-mixing calculation for all Nilsson levels originating from the $N = 4$ harmonic-oscillator shell. This calculation shows that, for the higher-spin members of the positive-parity rotational-like sequence, a decoupled band structure develops on top of the $2d_{5/2}$ and $1g_{7/2}$ single-particle orbits. This structure becomes more pronounced when the strong coupling wave functions are transformed to a basis where the core angular momentum is a good quantum number. In this way, the wave functions obtained from band mixing of Nilsson orbitals compare, even in detail, with the wave functions resulting from the unified-model calculations. This equivalence has in some places been traced back to identical expressions that result from either the core-coupling model (Alaga model) or from the Nilsson model. A more detailed study of this equivalence, with application especially to the odd-mass In isotopes, will be published.

The authors are indebted to Professor A. J. Deruytter for his interest during the course of this work and to N. Smith and A. A. Delucchi of LLL for performing the necessary chemical separations. We wish to acknowledge the beneficial discussions we have had with Dr. A. K. Kerman, Dr. J. O. Rasmussen, Dr. F. S. Stephens, Dr. R. M. Diamond, Dr. W. B. Walters, Dr. A. Bäcklin, Dr. G. L. Struble, Dr. F. S. Dietrich, and Dr. R. G. Markham. One of the authors (K.H.) is grateful to Professor R. Chery for his kind hospitality at the IPN (Lyon) and to J. Sau for illuminating discussions. Another author (R.A.M.) wishes to thank Dr. C. Gatrousis, Dr. W. Goishi, and Dr. D. G. Gardner, who first pointed to the problem in the odd-mass indium via inconsistencies in their calculations of isomer-ratio reaction cross sections versus experiment.

APPENDIX A

The matrix elements to be calculated in the secular equation (4.9) have been abbreviated into the following short-hand notations:

$$H(hR, H'R'; J) \equiv \langle j_h^{-1}, \mathrm{Sn}(R); J|_{\mathrm{h\ core}} | j_{h'}^{-1}, \mathrm{Sn}(R'); J\rangle , \tag{A1}$$

$$L(hR, p'I'i'; J) \equiv \langle j_h^{-1}, \mathrm{Sn}(R); J | V_{\mathrm{ph}} + H_{\mathrm{ph\ core}} | j_{p'}, \mathrm{Cd}(I', i'); J\rangle , \tag{A2}$$

$$K(pI\,i, p'I'i'; J) \equiv \langle j_p, \mathrm{Cd}(I, i); J | V_{\mathrm{ph}} + H_{\mathrm{p\ core}} | j_{p'}, \mathrm{Cd}(I', i'); J\rangle . \tag{A3}$$

Here R is used as a short-hand notation for the quantum numbers specifying the collective states: $(N_q R_q, N_0 R_0)R$. In all following formulas, $\hat{I}$ stands for $(2I+1)^{1/2}$.

Following we give the full expression for the matrix elements (A2) and (A3). The matrix element giving the coupling between single-particle states outside of the $Z = 50$ closed shell and excitations of the doubly-even Cd nucleus, can be described in a two-hole-core (Sn) unified-model calculation [Eqs. (4.3) and (4.4)] by

$$K(pIi,p'I'i';J)=\sum_{\substack{h_1,h_2,J_c,\\ h_1',h_2',J_c',\\ R,R',J_1}} d^{(i)}[(h_1h_2)J_c,R;I]d^{(i')}[(h_1'h_2')J_c',R';I']\times(2J_1+1)\hat{I}\hat{I}'\delta_{R,R'}\begin{Bmatrix} j_p & J_c & J_1\\ R & J & I\end{Bmatrix}\begin{Bmatrix} j_{p'} & J_c' & J_1\\ R' & J & I'\end{Bmatrix}$$

$$\times\langle(j_{h_1}j_{h_2})J_c;j_p;J_1|V_{ph}|(j_{h_1'}j_{h_2'})J_c',j_{p'};J_1\rangle+\delta_{h_1h_1'}\delta_{h_2h_2'}\delta_{J_cJ_c'}(-1)^{j_p+j_{p'}-I-I'+2J}$$

$$\times\begin{Bmatrix} j_p & R & J_1\\ J_c & J & I\end{Bmatrix}\begin{Bmatrix} j_{p'} & R' & J_1\\ J_c' & J & I'\end{Bmatrix}\langle j_p,\mathrm{Sn}(R);J_1|H_{p\,\mathrm{core}}|j_{p'},\mathrm{Sn}(R');J_1\rangle|. \tag{A4}$$

The separate contributions of the matrix elements describe the particle-core (Sn) coupling interaction and the residual particle-hole interaction. Expressions for the 1p-2h matrix element are not given here, but the result can be obtained as a limiting situation of the K matrix element as defined in Eq. (9e) of Ref. 53 with $u_a=u_b=u_d=u_e=0$, $u_c=u_f=1$. If we consider only the $(1g_{9/2}{}^{-2})_{0^+}$ two-hole configuration in connecting the collective states in Cd and Sn,[5] then Eq. (A4) reduces to Eq. (4.10). The matrix element connecting the subsystems of the secular equation (4.9) where single-hole-core (Sn) coupled configurations and single-particle-core (Cd) coupled configurations occur reads

$$L(hR,p'I'i';J)=\sum_{\substack{h_1',h_2',J'\\ R',J_1}} d^{(i')}[(h_1'h_2')J_c',R';I']|\hat{J}_1\hat{I}'(-1)^{R+J-J_1}$$

$$\times\begin{Bmatrix} j_{p'} & J_c' & J_1\\ R & J & I'\end{Bmatrix}2\left(\frac{2J_c'+1}{2J_1+1}\right)^{1/2}G(j_{h_1'},j_{h_2'},j_{p'}J_1;J_c')(1+\delta_{h_1'h_2'})^{-1/2}\delta_{RR'}$$

$$\times\delta_{J_1j_h}-(-1)^{j_{p'}+J_h+J_c'+R+R'-\lambda}(2J_1+1)\hat{I}'\hat{J}_c'\begin{Bmatrix} j_{p'} & J_c' & J_1\\ R & J & I'\end{Bmatrix}\begin{Bmatrix} j_h & R & J\\ R' & J_1 & \lambda\end{Bmatrix}$$

$$\times\left(\langle j_{h_1'}\|Y_\lambda\|j_{p'}\rangle\begin{Bmatrix} j_h & \lambda & J_1\\ j_{p'} & J_c' & j_{h_1'}\end{Bmatrix}\delta_{hh_2'}-(-1)^{j_h+j_{h_2'}-J_c'}\langle j_{h_2'}\|Y_\lambda\|j_{p'}\rangle\right.$$

$$\left.\times\begin{Bmatrix} j_h & \lambda & J_1\\ h_{p'} & J_c' & j_{h_2'}\end{Bmatrix}\delta_{hh_1'}\right)(1+\delta_{h_1'h_2'})^{-1/2}(\xi_\lambda\hbar\omega_\lambda)_{\mathrm{Sn}}\langle R\|b_\lambda+b_\lambda^\dagger\|R'\rangle|. \tag{A5}$$

[The precise definition of the G and F matrix elements occurring in Eqs. (A5), (4.10), and (4.11) is also found in Ref. 53.]

Again, the contributions from V_{ph} and $H_{ph\,core}$ are clearly separated. Contributions from V_{ph} will always be very small because of the condition $\vec{j}_{p'}+\vec{j}_h=\vec{J}_c'$; and because mainly $1\hbar\omega$ excitations through the $Z=50$ proton shell are considered, only a few terms from the $2\hbar\omega$ excitations $(1h_{11/2},2p_{3/2}{}^{-1},2p_{1/2}{}^{-1},1f_{5/2}{}^{-1})$ will contribute. If the approximation of only considering $(1g_{9/2}{}^{-2})_{0^+}$ configurations[5] is made in connecting collective excitations in Cd and Sn, expression (A5) simplifies into Eq. (4.11).

APPENDIX B

The reduced-transition matrix element from an initial state $|J_i^\alpha M_i\rangle$ to the final state $|J_f^\beta M_f\rangle$, with wave functions described by Eq. (4.8) and with the electromagnetic operators as indicated in Eqs. (5.6) and

(5.7), can be calculated to be

$$\langle J_f^\beta M_f \| O_{\lambda\mu} \| J_i^\alpha M_i \rangle = \sum_{\substack{h,h' \\ R,R'}} h^\alpha(hR; J_i) h^\beta(h'R'; J_f)(-1)^{j_{h'}+R'+\lambda}$$

$$\times \hat{J}_i \hat{J}_f \Big| (-1)^{J_i+\lambda+1} \langle j_{h'} \| O_{\lambda\mu}(\text{s.p.}) \| j_h \rangle \begin{Bmatrix} j_h & J_f & R' \\ J_i & j_h & \lambda \end{Bmatrix} \delta_{RR'}$$

$$+ (-1)^{J_f} \langle R' \| b_\lambda + b_\lambda^\dagger \| R \rangle B(E\lambda; \lambda \to 0_1^+)_{\text{Sn}}^{1/2} \begin{Bmatrix} R' & J_f & j_{h'} \\ J_i & R & \lambda \end{Bmatrix} \delta_{hh'} \Big|$$

$$+ \sum_{\substack{p,I,i \\ h',R',\{O\}}} p^\alpha(pIi; J_i) h^\beta(h'R'; J_f) d^{(i)}[(h_2 h_2)J, R; I] \hat{J}_i \cdot \hat{J}_f$$

$$\times \sum_{J_1} \hat{I}\hat{J}_1 \begin{Bmatrix} j_p & J & J_1 \\ R & J_i & I \end{Bmatrix} (-1)^{\lambda - J_1 + j_{h'}} \begin{Bmatrix} j_{h'} & J_f & R \\ J_i & J_1 & \lambda \end{Bmatrix} \langle j_{h'} \| O_{\lambda\mu}(\text{s.p.}) \| (j_{h_1} j_{h_2})J, j_p; J_1 \rangle$$

$$\times \delta_{RR'} + [\alpha \rightleftarrows \beta; \text{primed} \rightleftarrows \text{unprimed}] \; (-1)^{J_i - J_f}$$

$$+ \sum_{\substack{p,I,i \\ p',I',i' \\ \{O,O'\}}} p^\alpha(pIi; J_i) p^\beta(p'I'i'; J_f) d^{(i)}[(h_1 h_2)J, R; I] d^{(i')}[(h_1', h_2')J', R'; I']$$

$$\times \hat{J}_i \hat{J}_f \Big| \sum_{J_1} (2J_1+1) \hat{I}\hat{I}' \begin{Bmatrix} j_p & J & J_1 \\ R' & J_f & I' \end{Bmatrix} \begin{Bmatrix} j_p & J & J_1 \\ R & J_i & I \end{Bmatrix} \begin{Bmatrix} R' & J_f & J_1 \\ J_i & R & \lambda \end{Bmatrix} (-1)^{R'+\lambda+J_i+J_1}$$

$$\times \langle R' \| b_\lambda + b_\lambda^\dagger \| R \rangle B(E_\lambda; \lambda \to 0_1^+)_{\text{Sn}}^{1/2} \delta_{pp'} \delta_{h_1 h_1'} \delta_{h_2 h_2'} \delta_{JJ'}$$

$$+ \sum_{J_1', J_1'} \hat{J}_1 \hat{J}_1' \hat{I}\hat{I}' (-1)^{R+J_f+J_1+\lambda} \begin{Bmatrix} J_1' & J_f & R' \\ J_i & J_1 & \lambda \end{Bmatrix} \begin{Bmatrix} j_{p'} & J' & J_1' \\ R' & J_f & I' \end{Bmatrix} \begin{Bmatrix} j_p & J & J_1 \\ R & J_i & I \end{Bmatrix}$$

$$\times \langle (j_{h_1'} j_{h_2'})J', j_{p'}; J_1' \| O_{\lambda\mu}(\text{s.p.}) \| (j_{h_1} j_{h_2})J, j_p; J_1 \rangle \delta_{RR'} \Big| . \tag{B1}$$

(Here we denote all quantum numbers for the final state with a prime.)

With $O_{\lambda\mu}(\text{s.p.})$, we denote the single-particle component of the electromagnetic multipole operator, and the symbolic summation index $\{O\}$ stands for all quantum numbers $\{h_1, h_2, J, R\}$. In the transition matrix element Eq. (B1), one observes three contributions: the single-hole and collective transitions in the hole-core (Sn) coupled system; the single-particle transition connecting both systems; and the single-particle and collective transition in the particle-core (Cd) coupled system. If we take again the $(1g_{9/2}^{-2})_{0^+}$ configuration as the most important in connecting the collective excitations in Cd and Sn [Ref. 5], Eq. (B1) reduces considerably, especially for the third contribution. The single-particle matrix elements $\langle \| O_{\lambda\mu}(\text{s.p.}) \| \rangle$ are not given explicitly but can similarly be obtained from the analogous equations [(A6) and (A8)] of Ref. 53 by taking into account the appropriate occupation probabilities.

The transition matrix element for the collective part of the magnetic-dipole operator then becomes

$$\sum_{h,R} h^{\alpha}(hR;J_i)h^{\beta}(h'R';J_f)\hat{J}_i\hat{J}_f(-1)^{j_h+R+J_f+1}[R(R+1)(2R+1)]^{1/2}\begin{Bmatrix} R' & J_f & j_{h'} \\ J_i & R & 1 \end{Bmatrix}\delta_{RR'}\delta_{hh'}$$

$$+\sum_{\substack{p,I,i \\ p',I'i' \\ \{o,o'\}}} p^{\alpha}(pIi;J_i)p^{\beta}(p'I'i';J_f)d^{(i)}[(h_1h_2)J,R;I]d^{(i')}[(h_1h_{2'})J',R';I']$$

$$\times\hat{J}_i\hat{J}_f\Bigg|\sum_{J_1}(2J_1+1)\hat{I}\hat{I}'\begin{Bmatrix} j_p & J & J_1 \\ R & J_i & 1 \end{Bmatrix}\begin{Bmatrix} j_p & J & J_1 \\ R & J_f & 1 \end{Bmatrix}(-1)^{J_i+J_1+R+1}[R(R+1)(2R+1)]^{1/2}$$

$$\times\begin{Bmatrix} R & J_f & J_1 \\ J_i & R & 1 \end{Bmatrix}\delta_{\{oo'\}}\delta_{II'}g_R\Bigg|. \tag{B2}$$

With the simplification $(1g_{9/2}{}^{-2})_{0^+}$, the second term of (B2) reduces to the collective $M1$ transition matrix element, as defined in the particle-core (Cd) system treated in an empirical way, because $g_R=(Z/A)_{Sn}\cong(Z/A)_{Cd}$.

---

†Work performed in part under the auspices of the U.S. Energy Research and Development Administration, contract No. W-7405-Eng-48.

*Aangesteld navorser of the NFWO.

[1]B. I. Atalay and L. W. Chiao-Yap, Phys. Rev. C 5, 369 (1972).
[2]S. Sen, Nucl. Phys. A191, 29 (1972).
[3]A. Covello, V. R. Manfredi, and A. Azzis, Nucl. Phys. A201, 215 (1973).
[4]H. J. Mang, F. Krmpotic, and S. M. Abecasis, Z. Phys. 262, 39 (1973).
[5]S. M. Abecasis, O. Civitarese, and F. Krmpotic, Phys. Rev. C 9, 2320 (1974).
[6]F. Iachello and J. W. Smits, Kernfysisch Versneller Instituut, University of Groningen, Groningen, Netherlands, annual report, 1973 (unpublished), p. 65.
[7]F. S. Dietrich, B. Herskind, R. A. Naumann, R. G. Stokstad, and G. E. Walker, Nucl. Phys. A155, 209 (1970).
[8]A. Bäcklin, B. Fogelberg, and S. G. Malmskog, Nucl. Phys. A96, 539 (1967).
[9]V. Sergeev, J. Becker, L. Eriksson, L. Gidefeldt, and L. Holmberg, Nucl. Phys. A202, 385 (1973).
[10]A. Marcinkowiski, A. Bäcklin, and I. Bergquist, Nucl. Phys. A179, 781 (1972).
[11]H. E. Bosch, J. Davidson, V. Silbergleit, C. A. Heras, and S. M. Abecasis, Z. Phys. 273, 373 (1975).
[12]C. W. Tang, A. Pakannen, Z. C. Mewter, C. D. Coryell, G. Chiloski, K. Bos, and A. H. Wapstra, Z. Phys. A272, 301 (1975).
[13]W. Dietrich and A. Bäcklin, Z. Phys. A276, 133 (1976).
[14]H. J. Kim, R. L. Robinson, and C. H. Johnson, Phys. Rev. 180, 1175 (1969).
[15]J. McDonald, B. Fogelberg, A. Bäcklin, and Y. Kawase, Nucl. Phys. A224, 13 (1974).
[16]W. K. Tuttle, III, P. H. Stelson, R. L. Robinson, W. T. Milner, F. K. McGowan, S. Raman, and W. K. Dagenhart, Phys. Rev. C 13, 1036 (1976).
[17]H. J. Kim and R. L. Robinson, Phys. Rev. C 9, 767 (1974).
[18]J. McDonald, P. Porter, and D. T. Stewart, Nucl. Phys. A104, 525 (1967).
[19]E. M. Bernstein, G. G. Seaman, and J. M. Palms, Nucl. Phys. A141, 67 (1970).
[20]R. S. Raghavan and P. Raghavan, Phys. Rev. Lett. 28, 54 (1972).
[21]H. Haas and D. A. Shirley, Lawrence Livermore Laboratory Report No. UCRL-20426, 1970 (unpublished).
[22]E. Thurière, Ph.D. thesis, University of Paris, Orsay, 1970 (unpublished).
[23]M. Conjeand, S. Harar, and E. Thuriere, Nucl. Phys. A129, 10 (1969).
[24]S. Harar and R. N. Horoshko, Nucl. Phys. A183, 161 (1972).
[25]R. G. Markham and H. W. Fulbright, Phys. Rev. C 9, 1633 (1974).
[26]G. Alaga, F. Krmpotic, and V. Lopac, Phys. Lett. 24B, 537 (1967).
[27]G. Alaga, in *Nuclear Structure and Nuclear Reactions*, edited by M. Jean and R. A. Ricci (Academic, New York, 1959), p. 28.
[28]A. Bohr and B. R. Mottelson, *Nuclear Structure Vol. I* (Benjamin, New York, 1969); *Nuclear Structure Vol. II* (Benjamin, New York, 1975).
[29]C. K. Ross and R. K. Badhuri, Nucl. Phys. A196, 369 (1972).
[30]W. H. A. Hesselink, B. R. Kooistra, L. W. Put, R. H. Siemssen, and S. Y. Van Der Werf, Nucl. Phys. A226, 229 (1974).
[31]J. W. Smits, W. H. A. Hesselink, F. Iachello, R. H. Siemssen, and A. Van Der Woude, in *Proceedings of the International Conference on Nuclear Physics, Munich, 1973*, edited by J. de Boer and H. J. Mang (North-Holland, Amsterdam, American Elsevier, New York, 1973), p. 223.

[32]C. V. Weiffenbach and R. Tickle, Phys. Rev. C 3, 1668 (1971).
[33]A. H. Wapstra and N. B. Gove, Nucl. Data A9, 303 (1971).
[34]B. S. Reehal and R. A. Sorensen, Phys. Rev. C 2, 819 (1970).
[35]O. Beer, A. E. Behay, P. Lopato, Y. Terrien, G. Vallois, and K. K. Seth, Nucl. Phys. A147, 326 (1970).
[36]K. Heyde, M. Waroquier, P. Van Isacker, and H. Vincz, Phys. Lett. 64B, 135 (1976); K. Heyde, in *Proceedings of the International Conference on Nuclear Structure and Spectroscopy*, edited by H. P. Blok and A. E. L. Dieperink (Scholar's Press, Amsterdam, 1974), p. 186.
[37]V. R. Pandharipande, K. G. Prasad, and R. P. Sharma, Nucl. Phys. A104, 525 (1967).
[38]T. Badica, C. Ciortea, S. Dima, A. Gelberg, A. Petrovici, and I. Popescu, Nucl. Phys. A222, 168 (1974); T. Badica, C. Cirotea, S. Dima, A. Gelberg, A. Petrovici, and I. Popescu, in *Proceedings of the International Conference on Nuclear Physics, Munich, 1973* (see Ref. 31), p. 146.
[39]G. F. Fuller and V. W. Cohen, Nucl. Data B9, Appendix 1 (1965).
[40]V. S. Shirley, in *Table of Nuclear Moments, Hyperfine Structure and Nuclear Radiations*, edited by E. Mathias and D. A. Shirley (North-Holland, Amsterdam, 1968).
[41]R. A. Meyer, in *Problems of Vibrational Nuclei*, edited by G. Alaga, V. Paar, and L. Sips (North-Holland, Amsterdam, 1975), Chap. 7, p. 40.
[42]W. Dietrich, A. Bäcklin, C. D. Lannergård, and I. Ragnarsson, Nucl. Phys. A253, 429 (1975).
[43]S. G. Nilsson, C. F. Tsang, A. Sobiczewski, Z. Szymanski, S. Wycech, C. Gustafson, I. L. Lamm, P. Möller, and B. Nilsson, Nucl. Phys. A131, 1 (1969).
[44]N. De Takacsy and S. Das Gupta, Nucl. Phys. A263, 237 (1976).
[45]N. De Takacsy and S. Das Gupta, Phys. Rev. C 13, 399 (1976).
[46]S. Das Gupta and N. De Takacsy, Am. J. Phys. 44, 47 (1976).
[47]R. O. Sayer, J. S. Smith, III, and W. T. Milner, At. Data Nucl. Data Tables 15, 85 (1975).
[48]M. Sakai, At. Data Nucl. Data Tables 15, 513 (1975).
[49]L. Silverberg, Ark. Fys. 20, 341 (1961).
[50]E. Baranger, in *Advances in Nuclear Physics*, edited by M. Baranger and E. Vogt (Plenum, New York, 1971), Vol. 4, p. 261.
[51]G. Vanden Berghe and K. Heyde, Nucl. Phys. A163, 478 (1971).
[52]V. Paar, Phys. Lett. 60B, 232 (1976); in *Heavy-Ion, High-Spin States and Nuclear Structure, Trieste, 1973* (IAEA, Vienna, 1975), p. 179; in *Problems of Vibrational Nuclei*, edited by G. Alaga, V. Paar, and L. Sips (North-Holland, Amsterdam, 1975), p. 15.
[53]T. T. S. Kuo, E. U. Baranger, and M. Baranger, Nucl. Phys. 79, 513 (1966).
[54]S. Raman and H. J. Kim, Nucl. Data Sheets 16, 195 (1975).
[55]E. L. Murri, L. D. Mc Isaac, and R. G. Helmer, Phys. Rev. 155, 1263 (1967).
[56]G. Graeffe, C. W. Tang, C. D. Coryell, and G. E. Gordon, Phys. Rev. 149, 884 (1966).
[57]M. Ishii, J. Phys. Soc. 32, 1450 (1972).
[58]A. Z. Hrynkiewicz, S. Ogaza, and M. Rybicka, Institute of Nuclear Physics Report No. 506/PL, 1966 (unpublished).
[59]M. M. Bajaj, S. L. Gupta, and N. K. Saha, Aust. J. Phys. 21, 317 (1968).
[60]J. L. Campbell and J. P. Kirk, Can. J. Phys. 47, 1257 (1969).
[61]R. A. Meyer, in *Proceedings of the ERDA Conference on x-Ray and Gamma-Ray Spectroscopy, Ann Arbor, Michigan, 1976* (Univ. of Michigan, Ann Arbor, 1976), Report CONF-670539.
[62]R. Gunnink and J. B. Niday, Lawrence Livermore Laboratory Report No. UCRL-51061, 1971–1972 (unpublished), Vols. I–IV.
[63]A. A. Delucchi and R. A. Meyer, Lawrence Livermore Laboratory Report No. DCRL-76615, 1974 (unpublished).
[64]A. A. Delucchi and R. A. Meyer, Bull. Am. Phys. Soc. 18, 703 (1973).
[65]R. A. Meyer and G. L. Struble, Bull. Am. Phys. Soc. 17, 651 (1972).
[66]R. A. Meyer, G. L. Struble, and N. Smith, Bull. Am. Phys. Soc. 18, 691 (1973).
[67]R. A. Meyer, J. T. Larsen, and R. G. Lanier, in *Proceedings of the International Conference on Nuclear Physics, Munich, 1973* (see Ref. 31), p. 131.
[68]R. A. Meyer and G. L. Struble, in *Proceedings of the International Conference on Nuclear Moments and Nuclear Structure*, edited by H. Horie and K. Sugimoto (J. Phys. Soc. Jpn. Suppl., 1972), p. 418.
[69]R. A. Meyer, in *Proceedings of the International Conference on Gamma-Ray Transition Probabilities*, Invited Lectures, Delhi, India (Univ. of Delhi, Delhi, India, 1974), Vol. 1.
[70]R. G. Markham and H. W. Fulbright, Nuclear Structure Research Laboratory, University of Rochester, Annual Report, 1972 (unpublished); and private communication.
[71]R. G. Markham and H. W. Fulbright, Bull. Am. Phys. Soc. 18, 99 (1973).
[72]P. H. Stelson, Oak Ridge National Laboratory, private communication.
[73]S. Raman and H. J. Kim, Nucl. Data B 5, 191 (1971).
[74]N. Smith, Lawrence Livermore Laboratory Report No. UCRL-14258, 1962 (unpublished).
[75]M. Glascock, S. V. Jackson, W. B. Walters, and R. A. Meyer (unpublished).
[76]K. Poggenberg, Oak Ridge National Laboratory, private communication.
[77]J. S. Merritt and F. H. Gibson, Atomic Energy of Canada, Ltd., Progress Report No. AECL-5315, 1975 (unpublished).
[78]C. M. Lederer, J. M. Hollander, and I. Perlman, *Table of Isotopes* (Wiley, New York, 1967), 6th ed.
[79]R. S. Hager and E. C. Seltzer, Nucl. Data A4, 1 (1968).
[80]C. M. Lederer, Lawrence Berkeley Laboratory Internal Document, 1972 (unpublished).
[81]N. B. Gove and M. J. Martin, Nucl. Data A10, 206 (1971).